



Effect of molecular conformation on the efficiency of the spin orbital charge recombination-induced intersystem crossing in bianthryls

Xiaoyu Zhao^{a,b}, Andrey A. Sukhanov^c, Kepeng Chen^b, Xinyu Geng^{a,b}, Yu Dong^b, Violeta K. Voronkova^c, Jianzhang Zhao^{a,b,*}, Lang Liu^{a,**}

^a Key Laboratory of Energy Materials Chemistry, Institute of Applied Chemistry, College of Chemistry, Xinjiang University, Urumqi, 830046, PR China

^b State Key Laboratory of Fine Chemicals, School of Chemical Engineering, Dalian University of Technology, 2 Ling Gong Road, Dalian, 116024, PR China

^c Zavoisky Physical-Technical Institute, FRC Kazan Scientific Center of Russian Academy of Sciences, Kazan, 420029, Russia

ARTICLE INFO

Keywords:

Bianthryl
Charge transfer
Intersystem crossing
Spin-orbit coupling
Triplet state

ABSTRACT

Two bianthryl dyads, with the two units connected at either the 2- or 9- positions of the anthryl moiety, were studied to establish the relationship between orientation of the anthryl moieties and the electronic coupling and intersystem crossing (ISC) efficiency. The anthryl moieties in the two dyads adopt a close-to-orthogonal geometry, with dihedral angles of 90° (9,9'-bianthryl) and 106° (2,9'-bianthryl) at the ground state, respectively. The charge transfer (CT) emission efficiency and the fluorescence lifetimes are clearly dependent on the electronic coupling between the two anthryls, and stronger coupling lead to higher fluorescence quantum yields (34% vs. 9%) and shorter luminescence lifetimes (13.9 ns vs. 38.6 ns). The bianthryl with more orthogonal geometry shows higher singlet oxygen quantum yields Φ_{Δ} (9,9'-bianthryl, $\Phi_{\Delta} = 53\%$) than 2,9'-bianthryl ($\Phi_{\Delta} = 32\%$). Moreover, highly solvent polarity-dependent fluorescence emission and Φ_{Δ} were observed for the dyads ($\Phi_{\Delta} = 22\text{--}53\%$), which is different from the trend of the monomer anthracene, thus we propose the spin-orbit charge transfer ISC (SOCT-ISC) is responsible for the triplet state productions of the dyads. Interestingly, we found that inducing a heavy atom (Br) does not increase the ISC yield of anthracene. ISC in bianthryls was also confirmed with nanosecond transient absorption spectroscopy, the featured $T_1 \rightarrow T_n$ absorption at ca. 433 nm was observed, and the triplet state lifetime are long (9,9'-bianthryl, $\tau_T = 353 \mu\text{s}$; 2,9'-bianthryl, $\tau_T = 493 \mu\text{s}$, in acetonitrile).

1. Introduction

Triplet photosensitizers (PSs) are versatile compounds, which have been used for photocatalysis [1–4], photovoltaics [5,6], photodynamic therapy [5,7–11], and triplet–triplet annihilation (TTA)-induced photon upconversion [10,12–16]. Triplet PSs should show strong absorption of excitation light and efficient ISC [10]. ISC is an electron spin forbidden process, thus magnetic torque is required for the electron spin rephrasing or flip. The straight forward method to enhance the ISC is using the heavy atom effect [10,17–22]. Triplet PSs contain Br, I, Pt, Ir, Ru atoms belong to this category [23–28]. However, the heavy atom can shorten the triplet state lifetime, induces toxicity, and in some cases the ISC is inefficient even with heavy atoms directly attached to the π -conjugation core of the chromophore. Thus, heavy atom-free triplet PSs are of particular interest. However, from a point of view

photochemistry, it is elusive to achieve efficient ISC in heavy atom-free triplet PSs. Some methods have been developed to enhance the ISC in heavy atom-free compounds, for instance the compounds with $n\text{-}\pi \leftrightarrow \pi\text{-}\pi^*$ transitions (El Sayed Rule) [29], exciton coupling [30,31], energy matching S_1/T_n states [10,17], and molecules containing electron spin converter [32,33]. However, normally these compounds are with synthetically demanding molecular structures. Therefore, it is highly desired to develop efficient triplet PSs based on simple molecular structures.

Concerning this aspect, charge recombination (CR)-induced ISC in electron donor/acceptor dyads, which has been known for decades, is in particular of interest [34–38]. Initially, these dyads were used to mimic natural photosynthesis centers to attain long-lived CT states [35,37,39,40]. Given the chromophore (either the electron donor or acceptor) is with lower localized triplet state energy level than the CT state, then the

* Corresponding author. Key Laboratory of Energy Materials Chemistry, Institute of Applied Chemistry, College of Chemistry, Xinjiang University, Urumqi, 830046, PR China.

** Corresponding author.

E-mail addresses: zhaojzh@dlut.edu.cn (J. Zhao), liulang@xju.edu.cn (L. Liu).

<https://doi.org/10.1016/j.dyepig.2020.109121>

Received 19 October 2020; Received in revised form 21 December 2020; Accepted 22 December 2020

Available online 28 December 2020

0143-7208/© 2020 Elsevier Ltd. All rights reserved.

CR may induce ISC and the located excited (LE) triplet state will be populated. However, the triplet state yields (ISC quantum yields) of these molecular systems were normally not studied. High ISC yield is not expected for these dyads because of the radical pair ISC (RP ISC) mechanism of these molecular systems. RP ISC is achieved with the hyperfine coupling interaction, which is known to occur with slow kinetics [34,41]. On the other hand, the separation of the electron donor and acceptor in these conventional dyads is large, in order to reduce the electronic coupling between the donor and acceptor (to prolong the CT state lifetime), thus with the resulted extremely small electron exchange energy (J), the RP ISC becomes feasible [42–44]. However, the large separation of the electron donor and acceptor makes the synthesis of the compounds difficult. Unfortunately, shortening the linker will increase the electronic coupling between the electron donor and acceptor, which makes the electron exchange energy large, and the RP ISC is inhibited. Therefore, electron donor/acceptor dyads with more simple molecular structure and fast ISC kinetics are desired.

Recently, compact electron donor/acceptor dyads were reported to show efficient ISC [45–49]. In these dyads containing short linker between the electron donor and acceptor, the donor and acceptor adopt orthogonal geometry [46,48], thus the CR is accompanied with molecular orbital angular momentum change, which compensate the electron spin angular momentum change of the ISC, as a result, the CR in these dyads may enhance ISC because the angular momentum conservation is satisfied in the CR/ISC. One advantage of these dyads is the simple molecular structure, the donor and acceptor can be connected by a single bond, given the orthogonal geometry is achieved with molecular conformation restriction [45,46,48,50–53]. Moreover, due to the strong electronic coupling between the donor and acceptor, the electron transfer (both the photo-induced charge separation (CS) and the CR) is fast, thus a high ISC can be expected. To date Bodipy [51], perylene [54], perylenemonoimide [55] have been used as the visible light-harvesting chromophore, and anthryl [56], phenothiazine [52] and phenoxazine [57] have been used as the electron donors for construction of compact electron donor/acceptor dyads showing efficient ISC. These electron donor/acceptor dyads share a common feature, i.e. the electron donor/acceptor are with drastically different structure, and normally with different redox potentials. One of the disadvantages of this molecular structural profile is the low CT state energy level, as a result, the energy level of the triplet state, which is formed by CR, is intrinsically low (it should be lower than the CT state) [37]. Triplet state with higher energy level is beneficial for the applications in electron transfer and energy transfer. Thus, a molecular structural profile for compact electron donor/acceptor dyads showing higher CT state energy levels are desired.

Concerning this aspect, the 9,9'-bianthryl (9,9'-BA) attracted our attention. 9,9'-BA was intensively studied for its symmetry breaking charge transfer (SBCT) [58–62], as well as the LE and the CT dual emission [59]. Triplet state formation was observed [59]. The bianthryl (BA) analogues were also used for organic light emitting diodes [63], especially for the reverse ISC from higher triplet state (T_5 state) to the singlet state to harvest the triplet excitons [64]. Recently, 9,9'-BA was used for emission color-tunable triplet–triplet annihilation upconversion [65]. The solvent polarity dependency of the fluorescence emission of 9,9'-BA was studied previously, it was proposed that the emissive state of 9,9'-BA is a twisted intramolecular charge transfer (TICT) state, especially in polar solvents [66]. The charge recombination relaxation of the CT state leads to triplet state [59]. Based on the orthogonal geometry, we propose the ISC mechanism in BA should be the SOCT-ISC. Triplet PSs with the SOCT-ISC mechanism, and contain two identical chromophores, i.e. showing SBCT, was rarely reported previously [67, 68].

Although the BAs have been studied for a long time, however their ISC mechanisms and the photophysical processes are still in controversy to some extent. For instance, some studies suggest that the emissive state of 9,9'-BA in polar solvent such as acetonitrile (ACN), is not a

conventional charge transfer state, rather, it is a charge resonance state without any transfer of one electron from one anthryl subunit to another [61]. In some cases the triplet state of 9,9'-BA was studied with nano-second transient absorption (ns TA), but the wavelength range monitored for the TA spectrum is limited, and the triplet state lifetime was not reported [59]. Some BA analogues were also studied for their charge transfer [69–71], but the molecular structural profile is still the 9,9'-biaryl, molecular structures with other geometry were not thoroughly studied. It has been shown that the electronic coupling and geometry play important role in determination of the photophysical property of the electron donor/acceptor dyads [67].

In order to address the above challenges, herein we studied the photophysical properties of two BAs, one is the 9,9'-BA and another is the 2,9'-BA (Scheme 1), the study is focused on the ISC and the triplet state. The two BAs show different geometry, 9,9'-BA shows orthogonal geometry, whereas 2,9'-BA is expected to show more coplanar geometry. As such the electronic coupling magnitude between the two anthryl units will be different, the photophysical properties of the two BAs, especially the ISC, will be different as well. However, to the best of our knowledge, such comparison was not performed. 2,9'-BA was reported recently as a fluorescent emitter for TTA upconversion [65], but its ISC and triplet state property was not studied. The two BAs were studied with steady state and time-resolved spectroscopies and Density Functional Theory (DFT) computations.

2. Results and discussion

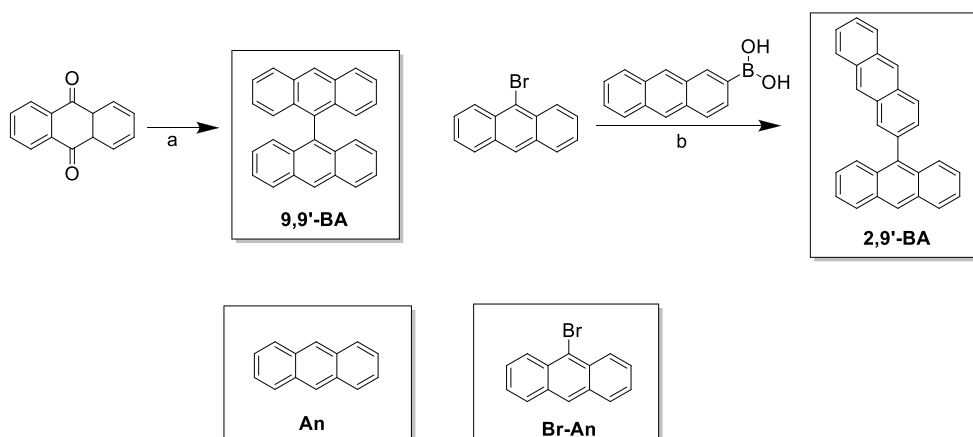
2.1. Design and synthesis of the compounds

9,9'-BA was known to adopt an orthogonal geometry [72,73], and TICT state was proposed for this BA, especially in polar solvent. In order to probe the relationship between the molecular geometry and the photophysical properties, especially the SOCT-ISC efficiency, 2,9'-BA was prepared (Scheme 1). During the preparation of this manuscript, 2,9'-BA was reported as a fluorescent emitter for triplet-triplet-annihilation upconversion (TTA-UC), but the ISC and the triplet state property was not studied [65]. The synthesis of 9,9'-BA is based on reductive coupling of 9-anthraquinone using zinc. The synthesis of 2,9'-BA is based on the Suzuki-Miyama crossing coupling reaction. The molecular structures were fully characterized by ^1H NMR, ^{13}C NMR and high resolution mass spectra (see ESI).

2.2. UV-Visible absorption and fluorescence emission spectra

The UV-Vis absorption of the compounds was studied (Fig. 1). The main absorption bands of BA derivatives are in the range of 300–425 nm, which are the structured absorption bands of the anthryl moiety. There is no obvious CT absorption band, indicating weak coupling between the two anthryl moieties at ground state, especially for 9,9'-BA [59]. However, for 2,9'-BA, the dihedral angle between two anthryl moieties is 106° (see Fig. 6), thus the electronic coupling is expected to be stronger than that in 9,9'-BA (dihedral angle: 90° , see Fig. 6). As a result, a broader absorption band was observed for 2,9'-BA (full width at half maximum (FWHM): 3950 cm^{-1}) than that of in 9,9'-BA (FWHM: 2110 cm^{-1}), which is probably due to the geometry distribution at the ground state and the stronger coupling between the two anthryl units. This is in agreement with the rotation potential energy studies (see later section).

Fluorescence emissions of the BA compounds were studied (Fig. 2). The fluorescence band of An is with significant vibrational progression, and the intensity and position are almost solvent polarity-independent (see ESI, Fig. S7a). However, the fluorescence bands of 9,9'-BA and 2,9'-BA are structureless and broad, especially in polar solvents (Fig. 2), and with increasing of the solvent polarity, the maximal emission wavelength are redshifted. In non-polar solvents, the emissive state is basically a LE state without significant CT feature, which was confirmed



Scheme 1. Reagents and conditions: (a) zinc powder, acetic acid, HCl, refluxed at 110 °C for 13 h under N₂, yield: 10%; (b) 2-anthraceneboronic acid, K₂CO₃, Pd(PPh₃)₄, toluene/ethanol/water, refluxed at 100 °C for 8 h, yield: 77%.

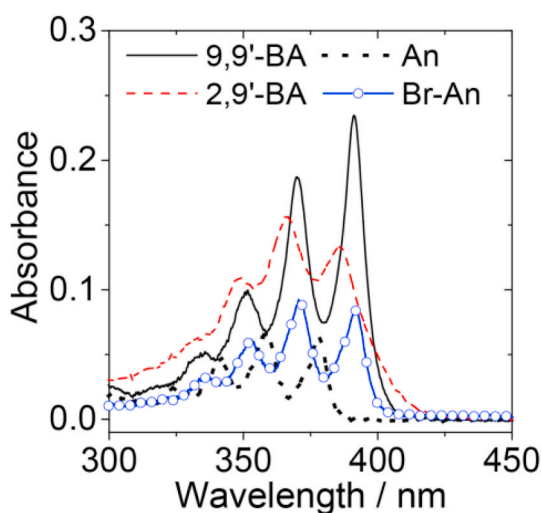


Fig. 1. UV-Vis absorption spectra of the compounds. $c = 1.0 \times 10^{-5}$ M in dichloromethane, 20 °C.

with femtosecond transient absorption spectroscopy [59]. However, it was proposed that even in non-polar solvent such as heptane, there is equilibrium between the LE state and a partially CT (PCT) state, based on time-resolved near IR absorption spectroscopy [74]. Thus the broad emission band of 9,9'-BA in *n*-hexane can be rationalized as the sum of a LE and PCT emission bands. In polar solvents, the emission intensity of BAs become weaker, which is the typical feature of the emissive excited state with significant charge transfer character [74,75]. It was also proposed that the broad emission bands are composed of two overlapping bands (LE emission and CT emission) [59]. In polar solvents, the PCT transfers to a fully charge separate state [74]. Based on femtosecond transient absorption spectroscopy, the charge separation in 9,9'-BA was determined as ca. 20 ps in alcohols [76]. In *N,N*-Dimethylformamide (DMF), the CS time constant was reported as 1.54 ps [65]. For 9,9'-BA, this spectral behavior was proposed as twisted ICT state [59,66,72,77,78]. Similar results were also observed for other 9,9'-biaryl compounds [69].

For 2,9'-BA, interestingly, the change of the fluorescence intensity with solvent polarity is less significant, which is in agreement with the recent study [65]. We propose that the CT state is with less extent of charge separation in 2,9'-BA, as compared in that of 9,9'-BA. The more significant solvent polarity-dependency of the emission of the 9,9'-BA should be attributed to the more significant CT feature of the S₁ state of

9,9'-BA than that of 2,9'-BA [59].

To study the effect of the magnitude of electronic coupling on the CT fluorescence profile, the electronic coupling matrix element between the ground state and CT state were calculated as using the following equation (1) [35,79].

$$V_{DA} (\text{cm}^{-1}) = \left[\frac{1.4 \times 10^5 k_r}{n^3 R_c^2 \nu_{\max}} \right]^{\frac{1}{2}} \quad (\text{eq. 1})$$

In eq. (1), $\nu_{\max} (\text{cm}^{-1})$ is position of the CT fluorescence maximum, $k_r (\text{s}^{-1})$ is the radiative rate constant, n is the solvent refractive index, and $R_c (\text{\AA})$ is the distance between the center of electron donor and acceptor, which was optimized by DFT calculations. R_c (9,9'-BA) = 4.35 Å and R_c (2,9'-BA) = 6.60 Å. The results are presented in Table 1. The V_{DA} values indicate the electronic coupling between the ground state and CT state [35], and the order of the electronic coupling extent for BA derivatives is 2,9'-BA > 9,9'-BA under low polarity solvents. But in highly polar solvent (i.e. ACN), electronic coupling extent is 9,9'-BA > 2,9'-BA, which manifests the stronger coupling in 9,9'-BA than in 2,9'-BA between ¹CT (after relaxation) and the ground state.

For electron donor/acceptor dyads with charge transfer emissive state, fluorescence is originated from either the LE state in non-polar solvents, or CT state in polar solvents. The former is featured with a structured emission band at shorter wavelength range, whereas the latter gives an emission band without fine structure, and in relatively red-shifted spectral region [75,80]. For 9,9'-BA, the fluorescence emission profile changes in different solvents in both aspects of emission intensity and emission wavelengths, which is more significant than that of 2,9'-BA. This result indicates that the excited dipole moment changes of 9,9'-BA is larger than that of 2,9'-BA. In order to quantitatively study the dipole moment of the emissive singlet excited states of the two dyads, the Stokes shift variation of the compounds in solvents with different polarity was analyzed with Lippert-Mataga equation (Fig. 2d and eq. (2)-(3) [75,81].

$$hc(\nu_a - \nu_f) = hc(\nu_a^0 - \nu_f^0) - \frac{2(\mu_e - \mu_g)^2}{a^3} f(\epsilon, n) \quad (\text{eq. 2})$$

$$f(\epsilon, n) = \frac{\epsilon - 1}{2\epsilon + 1} - \frac{n^2 - 1}{2n^2 + 1}, a = (3M/4N\pi d)^{\frac{1}{3}} \quad (\text{eq. 3})$$

where f is the orientational polarizability of solvents, μ_e is the excited-state dipole moment, μ_g is the ground-state dipole moment, a is the solvent cavity (Onsager) radius, derived from the Avogadro number (N), molecular weight (M), and density ($d = 1.0 \text{ g/cm}^3$), ϵ and n are the solvent dielectric and the solvent refractive index, respectively. The slopes of Lippert-Mataga plots indicate that the excited dipole moment

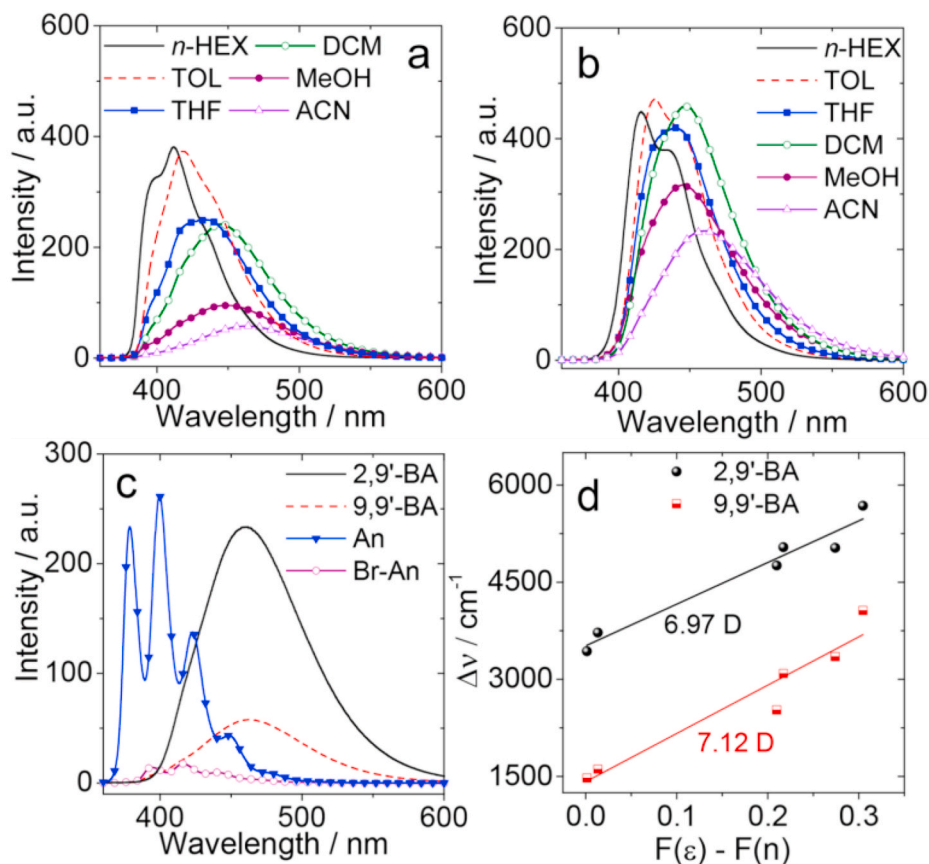


Fig. 2. Fluorescence emission spectra of (a) 9,9'-BA and (b) 2,9'-BA in different solvents. (c) Fluorescence emission spectra of 9,9'-BA, 2,9'-BA, An and Br-An in ACN, (d) Lippert–Mataga regressions of 9,9'-BA and 2,9'-BA. Optically matched solutions were used for all the measurements, ($\lambda_{\text{ex}} = 350 \text{ nm}$, $A = 0.093$), $20 \text{ }^\circ\text{C}$ (slight variation of the concentration is necessary to obtain optically matched solutions).

Table 1

Photophysical parameters of the compounds.

	solvent ^a	λ_{abs} ^b	ϵ ^c	λ_{em} ^d	τ_{F} ^e	Φ_{F} ^f	k_{r} ^g	k_{nr} ^h	V_{DA} ⁱ
9,9'-BA	TOL	392	2.4	418	$7.0^k/10.7^j$	60	8.6	5.7	0.10
	DCM	391	2.3	445	$17.2^k/26.7^j$	41	2.4	3.4	0.21
	ACN	389	2.4	462	$19.7^k/38.6^j$	9.0	0.5	4.6	0.35
2,9'-BA	TOL	367	1.6	425	$4.7^k/6.1^j$	77	16	4.9	0.20
	DCM	366	1.6	448	$5.6^k/9.9^j$	76	14	4.3	0.33
	ACN	364	1.5	459	$8.0^k/13.9^j$	34	4.3	8.3	0.33
An	TOL	359	0.7	403	$3.3^k/4.0^j$	30	9.1	21	— ^l
	DCM	358	0.7	402	$2.2^k/2.3^j$	16	7.3	38	— ^l
	ACN	356	0.6	399	$3.9^k/5.0^j$	23	5.9	20	— ^l
Br-An	TOL	372	0.9	398	$0.3(98.7\%),$ $4.2(1.3\%)^k$	7.0	23	310	— ^l
	DCM	371	0.9	418	$0.3(99.8\%),$ $4.7(1.2\%)^k$	3.0	10	323	— ^l
	ACN	369	0.8	416	$0.2(99.2\%),$ $3.9(0.8\%)^k$	2.0	10	490	— ^l

^a $E_{\text{T}}(30)$ values of the solvents, in kcal mol^{-1} . TOL (33.9), DCM (40.7) and ACN (45.6), respectively.

^b $c = 1.0 \times 10^{-5} \text{ M}$, in nm.

^c Molar extinction coefficient at the absorption maxima. $\epsilon: 10^4 \text{ M}^{-1} \text{ cm}^{-1}$.

^d In nm, $\lambda_{\text{ex}} = 350 \text{ nm}$.

^e Fluorescence lifetimes ($\lambda_{\text{ex}} = 340 \text{ nm}$), in ns, $c = 1.0 \times 10^{-5} \text{ M}$.

^f Fluorescence quantum yields with anthracene as standard ($\Phi_{\text{F}} = 27\%$ in ethanol) in aerated, $\lambda_{\text{ex}} = 350 \text{ nm}$, in %.

^g Radiative decay rate constant, derived from fluorescence data $k_{\text{r}} = \Phi_{\text{F}}/\tau_{\text{F}}$, in 10^7 s^{-1} , in aerated solution.

^h Nonradiative rate constant $k_{\text{nr}} = (1 - \Phi_{\text{F}})/\tau_{\text{F}}$, in 10^7 s^{-1} , in aerated solution.

ⁱ The electronic coupling matrix element between the CT state and ground state, in cm^{-1} .

^j Measured in deaerated solutions.

^k Measured in oxygen-saturated solutions.

^l Not applicable.

of **9,9'-BA** (7.12 D) is larger than that of **2,9'-BA** (6.97 D), based on the ground state dipole moments of **9,9'-BA** (0 D) and **2,9'-BA** (0.36 D), obtained with the optimized ground state (S_0) geometry. Previously it was proposed the excited state dipole moment of **9,9'-BA** in polar solvent is up to 20 D [71].

For further study of charge transfer in BAs, we estimated the degree of electron transfer, using $\Delta\mu$ (the different between the ground state dipole moments and the excited state dipole moments) and R_c (the centroid-to distance between the electron donor and acceptor) [82]. For **9,9'-BA**, $R_c = 4.35 \text{ \AA}$ and $\Delta\mu = 7.12 \text{ D}$, a transfer of 0.87 electron happened from the one anthryl to another anthryl part. However, R_c (**2,9'-BA**) = 6.60 \AA , $\Delta\mu = 6.61 \text{ D}$ and 0.56 electron transferred in **2,9'-BA**, which indicated the more significant degree of electron transfer in **9,9'-BA**.

The fluorescence lifetimes of the compounds were studied (Fig. 3), with the time-correlated single photon counting (TCSPC) technique. Both dyads show normal fluorescence lifetimes in non-polar solvents such as *n*-hexane (*n*-HEX, ca. 6 or 7 ns). In more polar solvents, for instances dichloromethane (DCM) and ACN, however, the fluorescence lifetime prolonged significantly, for example, 26.7 ns in DCM and 38.6 ns in ACN were observed for **9,9'-BA**, respectively. The result is very close to the previously reported lifetime for **9,9'-BA** in ACN (35.26 ns) [59]. Previously it was reported the fluorescence decay of **9,9'-BA** in heptane ($E_T(30) = 31.1 \text{ kcal mol}^{-1}$) is $(13 \pm 1) \text{ ns}$, both the LE and the PCT state decay with the same lifetime [74]. In our case we observed a lifetime of 7.2 ns in *n*-HEX ($E_T(30) = 31.0 \text{ kcal mol}^{-1}$).

The fluorescence lifetimes of **2,9'-BA** show a similar trend, but to a lesser extent. For instance, the fluorescence lifetime is 6.2 ns in non-polar solvents, *n*-HEX. However, in more polar solvents, the fluorescence lifetime has no more significant extension like **9,9'-BA**, for example, 8.4 ns in DCM and 13.9 ns in ACN were observed, respectively. Recently the fluorescence of **2,9'-BA** was reported as 6.07 ns in toluene (TOL) and 11.81 ns in DMF [65]. Similar to that of **9,9'-BA**, we propose the prolonged fluorescence lifetimes of the dyads in polar solvents are due to forbidden feature of the radiative CT state. For **9,9'-BA**, the geometry of the S_1 state is more orthogonal in polar solvents ($\phi = 67^\circ$, based on the optimized excited state S_1 geometry in ACN), makes the $S_1 \rightarrow S_0$ more forbidden, thus the emission intensity decreased but the fluorescence lifetime is prolonged. It was proposed that the S_1 state is distorted from the Franck-Condon geometry, and the torsion between the two anthryl units is 70° [59,76].

For **2,9'-BA**, the prolonging of the lifetime in polar solvent is less significant, which is in agreement with the geometry of the dyad (less orthogonal geometry, $\phi = 132^\circ$, i.e. the two anthryl units are more coplanar than that of **9,9'-BA**), electronic coupling is stronger due to the

large spatial overlap of the HOMO and LUMO orbitals (Fig. 8). Thus the forbidden feature of the CT excited state is less in **2,9'-BA** [17].

Recently, the fluorescence intensity of 10,10'-diphenyl-9,9'-bianthracene was studied, on the reverse intersystem crossing (RISC) process in organic light emitting diodes (OLEDs) [64]. It was proposed that the different fluorescence intensity under different atmosphere (i.e. N_2 , air and O_2) is due to the exciton at the S_1 state on the orthogonal bianthracene can be transferred to T_1 and finally quenched by triplet oxygen [64]. However, we measured fluorescence intensity of **9,9'-BA** and **2,9'-BA** under N_2 , air and O_2 atmosphere in TOL and ACN (Fig. S8). It was found that the I_0/I_{100} values of **2,9'-BA** are 2.90 and 5.15 in TOL and ACN, respectively (where I_0 stands for the fluorescence intensity in inert atmosphere (i.e. N_2) and I_{100} stands for the fluorescence intensity in neat O_2). While those of **9,9'-BA** are 3.75 and 13.25, which are highly solvent dependent and it is more significant for **9,9'-BA** than **2,9'-BA**. Thus, we concluded that fluorescence intensity change is more likely to be caused by the difference of fluorescence lifetimes under different atmosphere. Longer fluorescence will cause more significant quenching by O_2 .

The photophysical properties of the compounds were summarized (Table 1). For **9,9'-BA**, the fluorescence property is more dependent on the solvent polarity as compared to **2,9'-BA**, in aspects of emission wavelengths and fluorescence quantum yields. For instance, the maximal emission wavelength of **9,9'-BA** is red-shifted from 418 nm in TOL to 462 nm in ACN, at the same time, the fluorescence quantum yields decreased from 60% to 9%. In comparison, **2,9'-BA** shows emission red-shift from 425 nm in TOL to 459 nm in ACN, accordingly the fluorescence quantum yields decreased from 77% to 34%. These results demonstrated the effect of the molecular geometry and the electronic coupling magnitude on the photophysical properties of the dyads.

Notably the fluorescence lifetime of 9-bromoAn (**Br-An**) ($\tau_F = 0.2 \text{ ns}$) is very short as compared to that of **An** ($\tau_F = 2.2\text{--}3.9 \text{ ns}$) and BAs ($\tau_F = 4.7\text{--}19.7 \text{ ns}$ in aerated solution) (Table 1). For instance, the fluorescence lifetime of **Br-An** in ACN is ca. 200 ps, very close to the previously reported 160 ps, determined with streak camera [83]. The sum of the fluorescence quantum yield and the singlet oxygen quantum yield is much smaller than unit, every different from that of the BAs [59]. Thus we propose there exist a non-radiative decay channel for **Br-An**, for instance the loose belt effect of the C-Br bond [17].

As an approximation of the ISC ability of the compounds, the singlet oxygen quantum yields (Φ_Δ) of the compounds were studied in detail (Table 2). For **An**, it is known the ISC is via the $S_1 \rightarrow T_2$ channel, both states share similar energy levels, which facilitate the ISC by enhance the coupling matrix elements and the density of states [84–86]. Interestingly, for **Br-An**, we did not observe any significant increase of the Φ_Δ values in the presence of heavy atom Br, but the fluorescence quantum

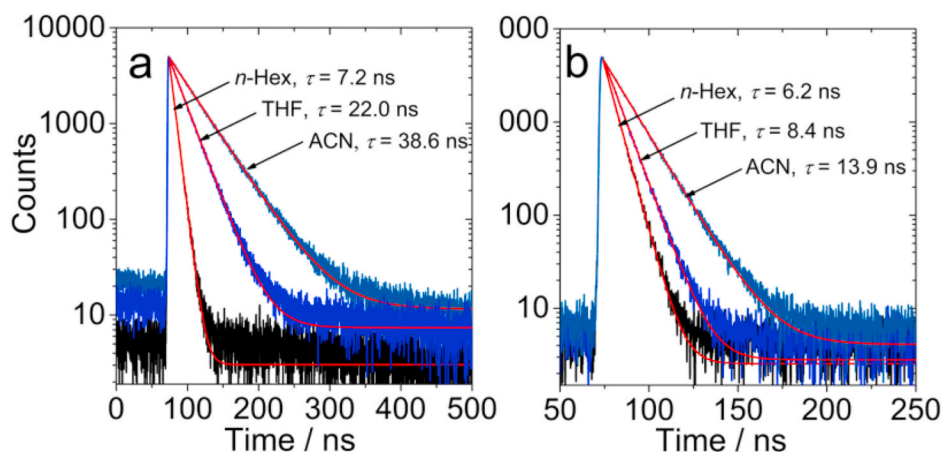


Fig. 3. Fluorescence decay curves of (a) **9,9'-BA** and (b) **2,9'-BA** in different deaerated solvents. $\lambda_{ex} = 340 \text{ nm}$ (EPL picosecond pulsed laser; TCSPC detection mode). For **9,9'-BA**, the monitored emission wavelengths are 412 nm (*n*-HEX), 446 nm (DCM) and 467 nm (ACN), respectively. For **2,9'-BA**, the monitored emission wavelengths are 416 nm (*n*-HEX), 448 nm (DCM) and 459 nm (ACN), respectively. $c = 1.0 \times 10^{-5} \text{ M}$, 20° C .

Table 2
Singlet oxygen quantum yields (Φ_{Δ} , in %) in different solvents ^a.

	<i>n</i> -HEX	TOL	THF	DCM	ACN	MeOH
9,9'-BA	21	22	24	27	53	26
2,9'-BA	21	15	18	12	32	20
An	20	52	28	65	51	18
Br-An	25	35	31	42	55	27

^a $E_T(30)$ values of the solvents, in kcal mol⁻¹. *n*-HEX (31.0), TOL (33.9), THF (37.4), DCM (40.7), ACN (45.6) and MeOH (55.4), respectively. Singlet oxygen quantum yield with [Ru(bpy)₃][PF₆]₂ as standard ($\Phi_{\Delta} = 57\%$ in DCM), in %, $\lambda_{ex} = 350$ nm.

yields decreased sharply as compared to that of **An** (Table 1). For both BAs, the Φ_{Δ} values are solvent polarity-dependent. For **9,9'-BA**, the highest Φ_{Δ} value was observed in ACN (53%), in other solvent, the Φ_{Δ} values are ca. 21–27%. We noted these results are different from the previous report on the solvent-dependency of the ISC quantum yield (based on ns TA method, the triplet state quantum yields were determined with relative method) [59]. But we believed that the singlet oxygen photosensitizing method is more convincing. For **2,9'-BA**, the Φ_{Δ} value is the highest in ACN (32%), in other solvents the Φ_{Δ} values are generally lower than that of **9,9'-BA**.

2.3. Redox properties: cyclic voltammogram of the compounds

In order to study the CS process, Gibbs free energy changes (ΔG_{CS}) of electron transfer as well as the energy level of the charge separated state (E_{CS}) in BA derivatives, the electrochemical properties of **9,9'-BA** and **2,9'-BA** were studied with cyclic voltammograms (CV, Fig. 4).

For **An**, an irreversible oxidation wave at +0.90 V and a reversible reduction wave at -2.40 V were observed, respectively (Fig. 4c). For **9,9'-BA**, a reversible oxidation wave at +0.88 V and.

A reversible reduction wave at -2.30 V were observed (Fig. 4a), which are different from **An**. However, for **2,9'-BA** (Fig. 4b), an oxidation wave at +0.92 V and a quasi-reversible reduction wave at -2.40 V (Table 3) were observed. The electrochemical properties of **9,9'-BA** was reported and the first reduction wave of **9,9'-BA** was $E(\text{red}) = -2.13$ V (vs Ag/AgCl) [87]. The bianthryl derivative (9,10-diphenylanthracene) was also reported at the same experiment conditions and showed reversible oxidation wave at +0.87 V and a reversible reduction wave at -2.26 V (vs Fc/Fc⁺) [88]. Thus, the redox potentials of BA dyads determined herein are reasonable.

The Gibbs free energy change (ΔG_{CS}) of the electron-transfer process was calculated using the Rehm-Weller equation (eq. (4)–6) [36,89],

$$\Delta G_{CS} = e[E_{OX} - E_{RED}] - E_{00} + \Delta G_S \quad (\text{eq. 4})$$

$$\Delta G_S = -\frac{e^2}{4\pi\epsilon_S\epsilon_0 R_C} - \frac{e^2}{8\pi\epsilon_0} \left(\frac{1}{R_D} + \frac{1}{R_A} \right) \left(\frac{1}{\epsilon_{REF}} - \frac{1}{\epsilon_S} \right) \quad (\text{eq. 5})$$

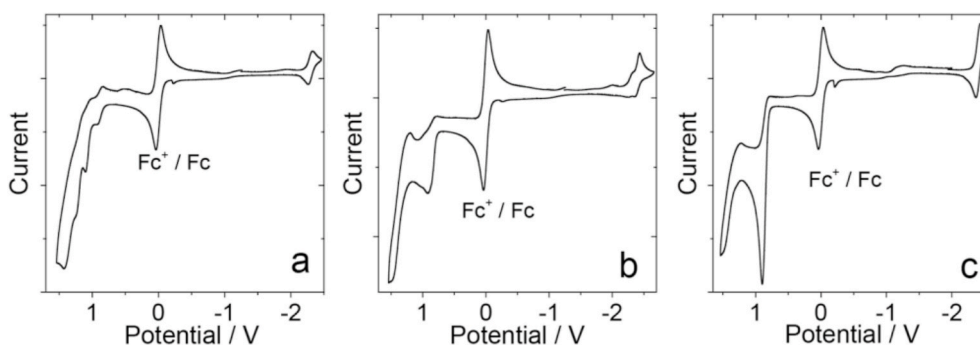


Fig. 4. Cyclic voltammograms of (a) **9,9'-BA**, (b) **2,9'-BA** and (c) **An** in deaerated ACN containing 0.10 M Bu₄N[PF₆] as the supporting electrolyte and Ag/AgNO₃ as the reference electrode. Scan rate: 100 mV/s. Ferrocene (Fc) was used as the internal reference, $c = 5.0 \times 10^{-4}$ M, 20 °C.

Table 3
Electrochemical redox potentials of the compounds ^a.

	$E(\text{ox})/\text{V}$	$E(\text{red})/\text{V}$	$E_{(\text{HOMO})}/\text{eV}^b$	$E_{(\text{LUMO})}/\text{eV}^c$
9,9'-BA	+0.88	-2.30	-5.66	-2.48
2,9'-BA	+0.92	-2.40	-5.70	-2.38
An	+0.90	-2.40	-5.68	-2.38

^a Cyclic voltammetry measurements in N₂-saturated ACN containing a 0.10 M Bu₄N[PF₆] supporting electrolyte. Redox potentials of the compounds were determined with ferrocene (Fc) as the internal standard (0 V). The counter electrode is the Pt electrode, the working electrode is the glassy carbon electrode, and the Ag/AgNO₃ couple is the reference electrode.

^b Calculated by $E_{(\text{HOMO})} = -4.78 + (E_{(\text{OX})}(\text{Fc}) - E_{(\text{OX})})$.

^c Calculated by $E_{(\text{LUMO})} = -4.78 + (E_{(\text{OX})}(\text{Fc}) - E_{(\text{RED})})$.

$$E_{CS} = e[E_{OX} - E_{RED}] + \Delta G_S \quad (\text{eq. 6})$$

in which ΔG_S is the static Coulombic energy, which is described by eq. (6). In eq. (4)–6, e is the electronic charge, E_{OX} is the half-wave potential for one-electron oxidation of the electron-donor unit (for irreversible oxidation, the anodic peak potential was used instead of the half-wave potential), and E_{RED} is the half-wave potential for one-electron reduction of the electron-acceptor unit, E_{00} is the energy level approximated with the crossing point of the normalized UV-Vis absorption and fluorescence emission spectra of anthracene (LE state), in *n*-HEX solution, ϵ_S is the static dielectric constant of the solvent, R_C is the center-to-center separation distance between the two anthracene moieties, determined by DFT optimization of the geometry, R_C (**9,9'-BA**) = 4.35 Å, R_C (**2,9'-BA**) = 6.60 Å, R_D is the radius of the electron donor, R_A is the radius of the electron acceptor, ϵ_{REF} is the static dielectric constant of the solvent used for the electrochemical studies, ϵ_0 is permittivity of free space. The solvents used in the calculation of free energy of the electron transfer is TOL ($\epsilon_S = 2.38$), DCM ($\epsilon_S = 8.93$) and ACN ($\epsilon_S = 37.5$).

The values of ΔG_{CS} indicated that the PET is thermodynamically allowed for all compounds listed in Table 4, and the driving forces for PET were larger in polar solvents (such as ACN) than in nonpolar solvents (such as TOL), which corresponds to the fluorescence changes. The energy levels of CT states are 3.14 eV (in DCM) and 3.09 eV (in ACN) for **9,9'-BA** (Table 4), which lie higher than ³An energy (1.78 eV). For **2,9'-BA**, the energy level of CT state is 3.26 eV in ACN. Moreover, the Gibbs free energy changes were calculated by eq. (4) (with the crossing point of the normalized UV-Vis absorption and fluorescence emission spectra of anthracene as the E_{00} values). The ΔG_{CS} of **9,9'-BA** are -0.13 eV (in DCM) and -0.18 eV (in ACN), and for **2,9'-BA** is -0.01 eV (in ACN), respectively, which indicates that the CS process driven is exoergic for **9,9'-BA** and **2,9'-BA** in polar solvent, but endergonic for **2,9'-BA** in solvents with moderate polarity (i.e. in DCM).

Table 4Gibbs free energy changes (ΔG_{CS}) for the intramolecular photo-induced electron transfer and CT state energy levels are presented ^a.

	ΔG_{CS} (eV)			E_{CS} (eV)				
9,9'-BA ^b	0.19 ^d	0.06 ^e	-0.13 ^f	-0.18 ^g	3.46 ^d	3.33 ^e	3.14 ^f	3.09 ^g
2,9'-BA ^c	1.05 ^d	0.68 ^e	0.14 ^f	-0.01 ^g	4.32 ^d	3.95 ^e	3.41 ^f	3.26 ^g

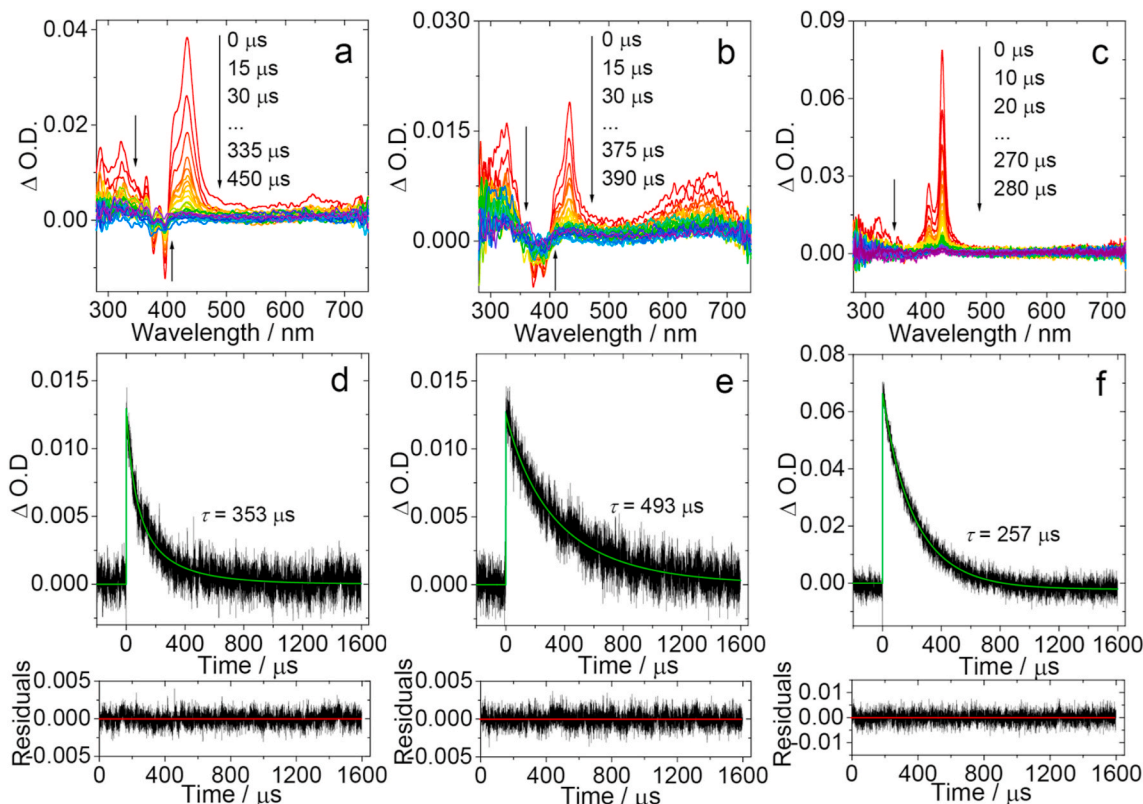
^a The redox potentials are approximated based on the redox potential measured in ACN.^b $E_{00} = 3.27$ eV.^c $E_{00} = 3.27$ eV. The energy levels of E_{00} are approximated with the crossing point of the normalized UV-Vis absorption and fluorescence emission spectra of anthracene, in *n*-HEX solution.^d In *n*-HEX.^e In TOL.^f In DCM.^g In ACN.

Fig. 5. Nanosecond time-resolved transient absorption spectra of (a) 9,9'-BA, (b) 2,9'-BA and (c) An ($\lambda_{ex} = 355$ nm). $c = 2 \times 10^{-5}$ M in deaerated ACN. Decay traces of (d) 9,9'-BA at 433 nm and (e) 2,9'-BA at 434 nm and (f) An at 427 nm ($\lambda_{ex} = 355$ nm) in deaerated ACN. The τ_T values in (d), (e) and (f) are the intrinsic lifetimes obtained by fitting the decay traces with the kinetic model by taking into account the TTA quenching effect (see ESI for details). The residues of the fittings are also shown.

2.4. Nanosecond transient absorption spectroscopy: the triplet excited state property of the compounds

In order to study the triplet excited state of the compounds, the nanosecond transient absorption spectra measurements were studied (Fig. 5). Upon pulsed laser excitation, a structured excited-state absorption (ESA) band centered 427 nm for An was observed (Fig. 5c), which is the typical absorption feature of the T_1 state of An [88]. With TDDFT computation, we assign this absorption band to $T_1 \rightarrow T_5$ transition (see ESI, Table S5 and Fig. S12 for orbitals involved in the transitions. The energy gap between T_1 and T_5 is 2.90 eV, based on the optimized T_1 state geometry). The intrinsic triplet state lifetime was determined as ca. 257 μ s (in ACN. Fitting of the decay traces with a kinetic model with the triplet-triplet annihilation quenching effect considered) [90]. The apparent triplet state lifetime is 59 μ s ($c = 2.0 \times 10^{-5}$ M, in deaerated ACN). It should be noted that for most of the reported triplet state

lifetimes, the effect of the TTA self-quenching was not considered, thus for the compounds showing efficient ISC and long triplet state lifetimes, the reported lifetimes are shorter than the intrinsic triplet state lifetime [90]. Previously the triplet state lifetime of An was reported as ca. 100 μ s [91]. It should be noted that the triplet state lifetimes of An varied significantly in different reports, in the range of 160–2900 μ s [92]. The efficient ISC (approximated with the singlet oxygen quantum yield, $\Phi_{\Delta} = 51\%$, in ACN) of An is attributed to the closely lying S_1/T_2 states, which share similar energies [84,88,93,94].

The ns TA spectrum of the BA shows a prominent ESA band centered at ca. 433 nm (Fig. 5a and b), which is similar but broader than that of An. From the molecular frontier orbital, T_1 state of 9,9'-BA is delocalized in the whole molecular. Furthermore, an ESA band at 1321 nm ($f = 0.169$, f is the Oscillator strengths) was predicted through TDDFT calculation, which is approximate to a literature report of an absorption band at 1250 nm of the CT state (in ACN), characterized by nanosecond

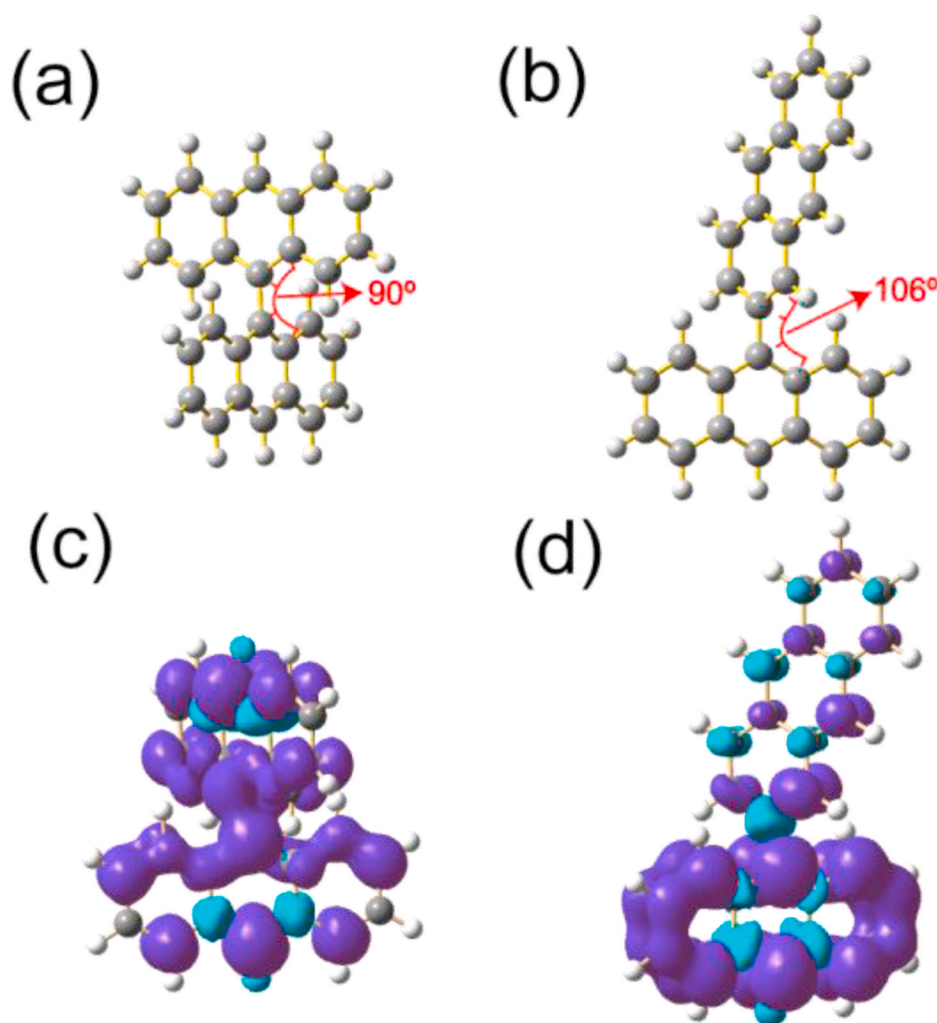


Fig. 6. Optimized ground state (S_0 state) geometries of (a) 9,9'-BA and (b) 2,9'-BA. The dihedral angles between two anthryl moieties are also presented. Spin density surfaces of the triplet excited state of (c) 9,9'-BA and (d) 2,9'-BA at the optimized triplet state geometry (Isovalue = 0.001). Calculated at B3LYP/6-31G (d) level with Gaussian 09W.

time-resolved near-IR spectroscopy [74]. These results imply that the triplet state of 9,9'-BA might be a special CT state with charge resonance character in polar solvents and different from the CT feature of the S_1 state [61,66,74]. The ns TA spectra of 9,9'-BA were studied previously [59], but not all the visible spectral range was monitored, and the triplet state lifetime was not reported. The intrinsic triplet state lifetime of 9,9'-BA was determined as 353 μ s in ACN (fitting based on the TTA model, Fig. 5d). The ESA bands of 9,9'-BA was calculated with TDDFT method, absorption bands at 307 nm, 358 nm and 452 nm were predicted in polar solvent (i.e. ACN), which are due to the $T_1 \rightarrow T_{30}$ ($f = 0.119$), $T_1 \rightarrow T_{22}$ ($f = 0.042$) and $T_1 \rightarrow T_{14}$ ($f = 0.164$) transitions between delocalized orbitals, respectively (see ESI, Table S2).

Recently 2,9'-BA was reported as a fluorescence emitter for TTA-UC, but the triplet state and the ISC property were not reported [65]. For 2,9'-BA, there is an ESA band centered as ca. 380 nm, which is in superimposition with the ground state bleaching (GSB) (Fig. 5b). A prominent ESA band centered at ca. 433 nm was also observed, which is similar to that of 9,9'-BA (Fig. 5a). From the molecular frontier orbital, the transition of T_1 state in 2,9'-BA belongs to HOMO \rightarrow LUMO, which is the feature of CT properties. Moreover, an ESA band at 940 nm ($f = 0.041$) was predicted through TDDFT calculation for 2,9'-BA. Therefore, we propose the triplet state of 2,9'-BA in polar solvent is also special CT state similar to that of 9,9'-BA. The triplet state lifetimes of 2,9'-BA were determined as 493 μ s (based on a kinetic model with triplet-triplet

annihilation self-quenching effect considered) [56,57]. The ESA bands of 2,9'-BA was calculated, absorption bands centered at 445 nm and 397 nm were predicted, which are due to the $T_1 \rightarrow T_{10}$ ($f = 0.386$) and $T_1 \rightarrow T_{24}$ ($f = 0.129$) transitions (see ESI, Table S4). These predictions are in good agreement with the experimental observations. The resulting configurations of $T_1 \rightarrow T_n$ were listed in supporting information (see ESI, Table S2, Table S4, Table S6 for 9,9'-BA, 2,9'-BA and An, respectively) And the comparison between the $T_1 \rightarrow T_n$ absorption bands based on TDDFT and experimental spectra were showed in supporting information (Fig. S12). To our knowledge, Castellano's group [95] and Beames's group [96] also calculate the $T_1 \rightarrow T_n$ absorption with same method, which are similar to experimental results.

2.5. DFT computations

The geometries of the bianthryl at the ground state were optimized (Fig. 6a and b). The dihedral angle between the two anthryl moieties in 9,9'-BA and 2,9'-BA are 90° and 106° , respectively. This orthogonal geometry of 9,9'-BA will make the two anthryl units electronically decoupled at ground state, which is in agreement with the UV-Vis absorption, in which no significant CT bands were observed (Fig. 1).

This is also in agreement with the long fluorescence lifetimes of 9,9'-BA in polar solvent (38.6 ns in ACN), because the TICT state is weakly emissive [75]. In comparison, 2,9'-BA is with more coplanar geometry,

thus the electronic coupling between the two anthryl units is stronger, the ICT state is more emissive, demonstrated by the higher fluorescence quantum yields and the shorter fluorescence lifetimes (Table 1).

The spin density surfaces of the triplet states of the dyads were computed (Fig. 6c and d), and it was found that the triplet state wave function is distributed over the whole molecule, i.e. both anthryl units, especially for 9,9'-BA. This is similar to the charge resonance mechanism proposed for the CT state of 9,9'-BA, confirmed with time-resolved near-IR transient absorption spectroscopy of the ^1CT state [61]. Interestingly, an absorption band at 1321 nm ($f = 0.169$) was also predicted in triplet state absorption for 9,9'-BA, based on TDDFT calculation, which is consistent with CT absorption bands centered at 1250 nm reported previously [61]. However, no similar triplet state absorption band were predicted for An, thus we supposed that ^3CT state have also the charge resonance character. We studied the time-resolved electron paramagnetic resonance (TREPR) spectra of 9,9'-BA, but no signal was observed. The degenerate triplet state on the two units in 9,9'-BA may be responsible for the fast SLR of the triplet state. For 2,9'-BA, the triplet state is more localized on one anthryl unit and the energy level difference is 0.5 eV between T_1 and T_2 . The anion and cation spin densities of the two compounds are also calculated, and the spin density surfaces are distributed on the whole molecule (see ESI, Fig. S11). These results are in agreement with the previously reported results that the CT state of the 9,9'-BA is not the conventional CT state [61].

In order to investigate the conformational constraints of the dyads for the torsion of the two anthryl units, the potential energy curves (PEC) of the rotation about the linker bonds were constructed (Fig. 7). For 9,9'-BA, the PEC is steeper than that of 2,9'-BA due to the large steric hindrance, as a result of the H atoms at peri-positions (i.e. the 1- and 8-position of the anthryl moiety) of the two anthryl units in 9,9'-BA. The geometries accessible with the thermal energy at room temperature are mainly with dihedral angles in the range of 79° – 100° for 9,9'-BA, however, it is 58° – 123° for 2,9'-BA (Fig. 7b), which indicates that 9,9'-BA prefers to take the orthogonal geometry. This situation is similar to the geometry isomers of the phenothiazine-anthracene dyads, i.e. the substitution at the 9-position is beneficial for conformation restriction than that at 2-position of the anthryl moiety [56]. The optimized S_0 state geometries show that the dihedral angle between the two anthryl moieties in 9,9'-BA is 90° , which is in agreement with literature reports [97, 98]. In addition, the dihedral angle of 2,9'-BA at ground state is 106° . However, molecules at the excited states (i.e. S_1 state and T_1 state, based on optimized excited state geometry) are more coplanar than ground state, for instance, the dihedral angles of 9,9'-BA at S_1 state and T_1 state are 67° and 119° , whereas they are 132° and 123° for 2,9'-BA. It was reported that the dihedral angle at S_1 state of 9,9'-BA between the two

anthryl units is 70° [59,76].

The frontier molecular orbitals of the BAs were studied for the ground state (S_0 state) and the S_1 state (Fig. 8). For 9,9'-BA, the HOMO and LUMO are fully delocalized on the two anthryl units, which is similar to the previous results obtained with semiempirical calculation [59]. For the optimized S_1 state geometry, however, the HOMO and LUMO are not equally distributed on the two anthryl units. It was proposed that the S_1 state is distorted from the Franck-Condon geometry, and the torsion between the two anthryl units is 70° [59,76]. This is in agreement with the CT feature of the S_1 state, especially in polar solvents. The MOs of the ground state and the S_1 state infer that the CT is a two-step process, i.e. firstly population of the LE Franck-Condon state, and then the CT state was formed, in other words, the CT state is not directly populated by photoexcitation. Based on femtosecond transient absorption spectroscopy, the charge separation in 9,9'-BA was determined as ca. 20 ps in alcohols [76], although different results were observed (1.54 ps in DMF) [65]. With time-resolved near-infrared absorption spectroscopy, the CS time constant was determined as ca. 0.3 ps (in heptane) [99]. The orthogonal LE state is unable to undergo CT, torsion is required for the FC state before the occurring of the CT [71].

For 2,9'-BA, however, the HOMO orbitals of the two anthryl units are not degenerated, the HOMO localized on the x-anthryl is with higher energy (-5.13 eV) than that on the y-anthryl unit (-5.32 eV). Interestingly, the LUMO localized on the x-anthryl is with lower energy (-1.76 eV) than the LUMO of the y-anthryl unit (-1.58 eV), where x-anthryl stands for the part of 9-position substituted anthryl, and y-anthryl stands for the part of 2-position substituted anthryl. The molecular orbitals of the ground state of 2,9'-BA indicate that CT absorption is possible, which is unlikely for 9,9'-BA. The UV-Vis absorption of 2,9'-BA was calculated with TDDFT method, transitions from $S_0 \rightarrow S_1$ at 422 nm ($f = 0.051$) and 400 nm from $S_0 \rightarrow S_2$ ($f = 0.035$) were predicted, which are assigned to the CT absorption, due to their smaller f value than LE absorption (385 nm), $S_0 \rightarrow S_3$ ($f = 0.127$) (see ESI, Table S3).

The photophysical properties of the compounds are summarized in Scheme 2. For An, it is known that the ISC is via the energy matching S_1/T_2 states (see ESI, Scheme S1) [88,93,94]. Experiments show it is also solvent-dependent (Table 1), which can be attributed to the variation of the S_1/T_2 state energy level by different solvents [100].

For the BAs, the scenario is more complicated, due to the formation of CT states. Steady state and time-resolved spectroscopies have demonstrated the formation of the CT state, especially in polar solvents for 9,9'-BA. Thus we expected contribution from the SOCT to the ISC, as well as the conventional SO-ISC for the anthryl, which is well known [101]. Note the SOCT-ISC efficiency is dependent on solvent polarity because the CT state energy levels, thus the matching of the CT state and

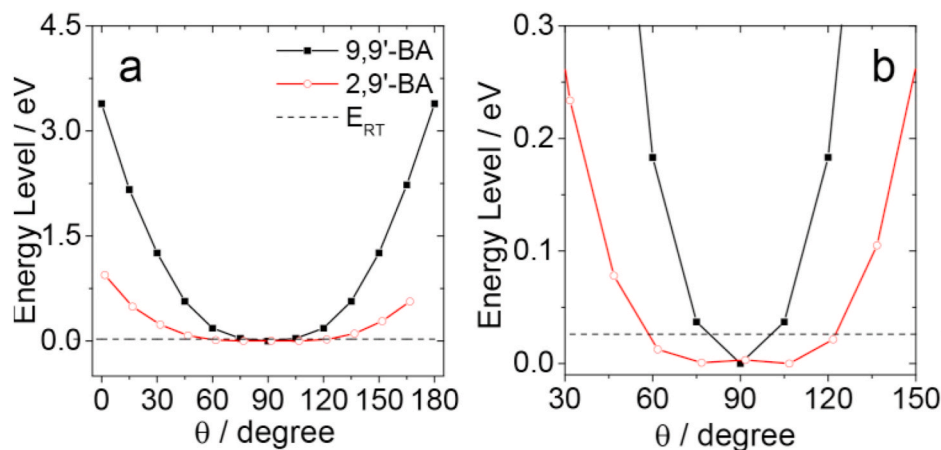


Fig. 7. B3LYP/6-31G (d) calculated potential energy curves of the rotation around the linker bond of 9,9'-BA and 2,9'-BA ground states. ϕ is the dihedral angle between two anthracene units at ground state. (b) Magnified low energy range of the potential energy surfaces near the minima. The thermal energy at room temperature ($E_{RT} = 0.026$ eV) is indicated by the dashed line.

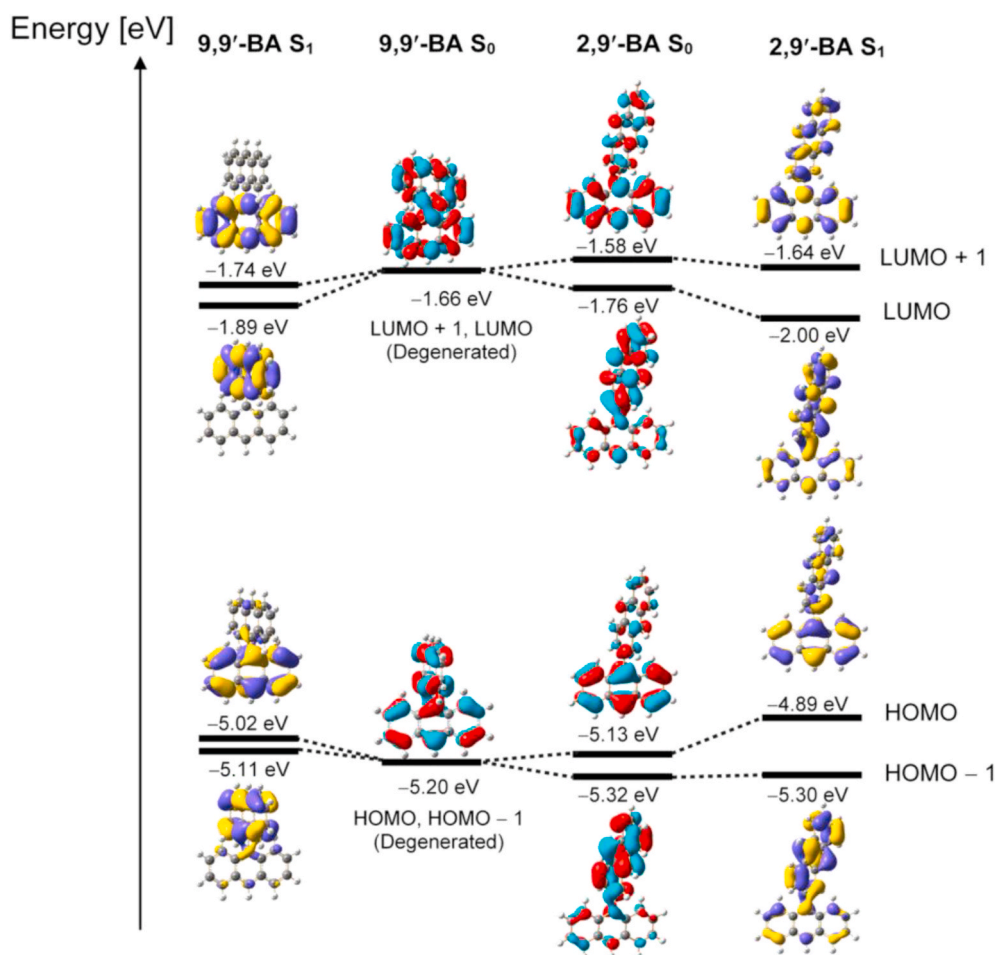


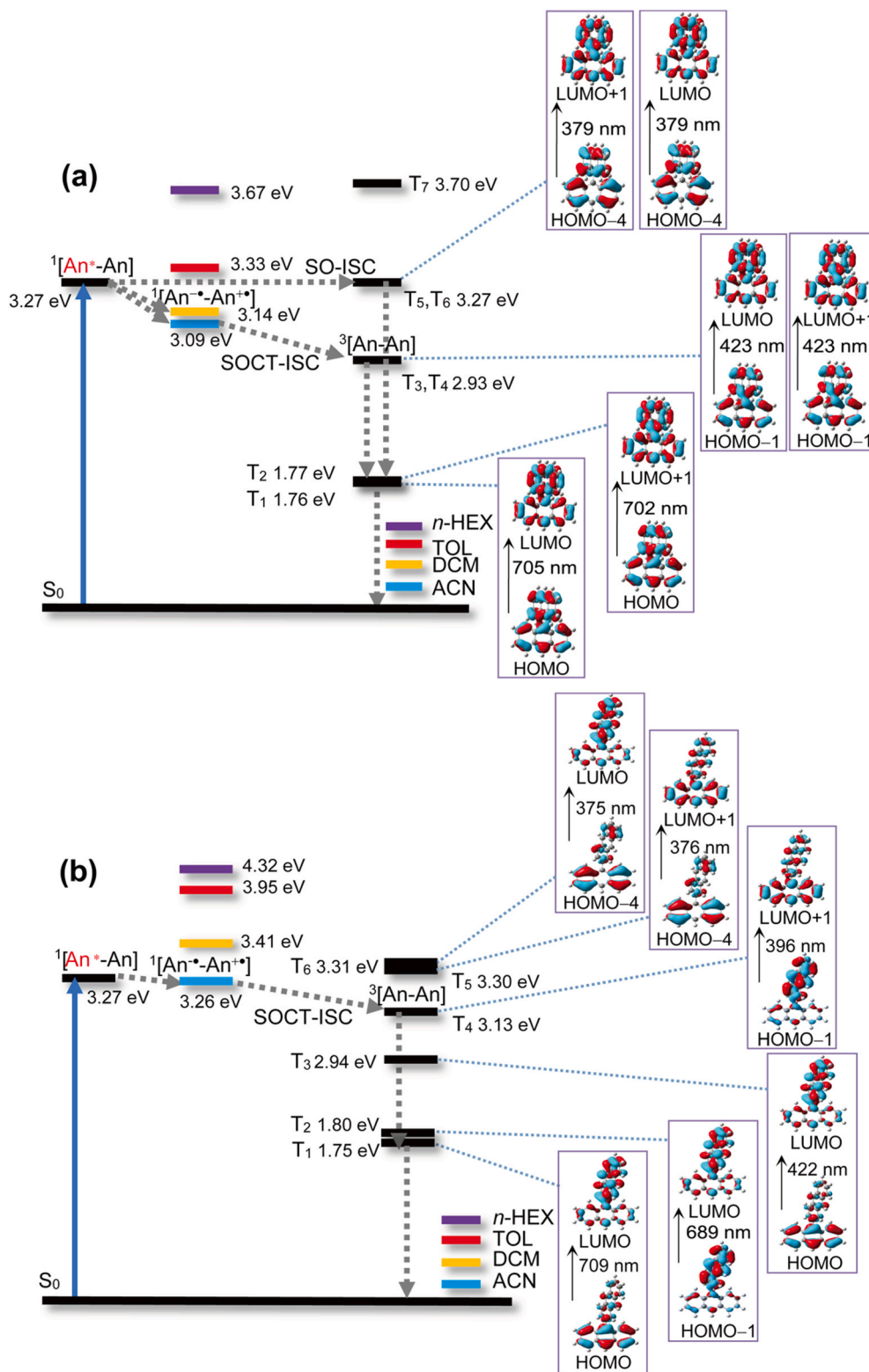
Fig. 8. The ground state (S_0) and the excited state (S_1) frontier molecular orbitals of 9,9'-BA and 2,9'-BA calculated by DFT (B3LYP/6-31G (d)) (Isovalue = 0.03). The energy levels of the orbits are presented (in eV).

the T_n state energy levels, are dependent on solvent polarity. Thus, the trend of the Φ_Δ of the compounds in different solvents varied for the two BAs and An. For instance, the Φ_Δ of 9,9'-BA, 2,9'-BA and An in TOL are 22%, 15% and 52%, respectively. For both BAs, the highest Φ_Δ were observed in ACN, but for An, the highest singlet oxygen quantum yield was observed in DCM. We propose the reason of the low ISC yield in 2,9'-BA is not only slow $^1[\text{An}^{\bullet-}\text{An}^{\bullet+}] \rightarrow T_4$ transition (both of $^1[\text{An}^{\bullet-}\text{An}^{\bullet+}]$ and T_4 possess the charge-transfer character), but also the effect of the molecular geometry, in which electron donor and acceptor adopt a more coplanar configuration. Based on SOCT-ISC mechanism, the orthogonal configuration between electron donor and acceptor will enhance ISC, due to the total angular momentum of the molecular system is conserved. However, the dihedral angle of 2,9'-BA at ground state is 106° , which is with more coplanar geometry, compared to 9,9'-BA (90°). Thus the more coplanar geometry in 2,9'-BA will lead to lower ISC yield than that of 9,9'-BA. TDDFT computation showed that after derivatization, the relative S_1/T_n energy levels changes as compared to that of An. For instance, there are degenerated T_3/T_4 states for 9,9'-BA, with 2.93 eV energy level, which is much lower than S_1 state (3.27 eV). In addition, degenerated T_3 , T_4 and degenerated T_5 , T_6 are both delocalized. This is different from An, for which the S_1/T_2 states are with energy levels of 3.27 eV and 3.23 eV, respectively. In *n*-HEX, the CS can be inhibited, but still moderate Φ_Δ were observed for 9,9'-BA (21%) and 2,9'-BA (21%), indicating ISC mechanisms other than SOCT-ISC exit for both BAs. The ISC rate constant of An is $(3 \pm 0.6) \times 10^8 \text{ s}^{-1}$ at room temperature [102], whereas the dynamics of TICT states is 3.2 ps for 2,9'-BA and 1.54 ps for 9,9'-BA in DMF, respectively [65]. Thus, SOCT-ISC should be faster than SO ISC in solvents with high polarity.

It should be noted the striking feature of the SBCT molecular systems is the high CT state energy levels [37]. For instance, we reported phenothiazine-anthracene compact electron donor/acceptor dyads showing SOCT-ISC previously [56], the CT states are with energy levels of 1.9–2.4 eV (with changing of the solvents from ACN to TOL). In comparison, the 9,9'-BA shows CT energy levels in the range of 3.1–3.3 eV (solvents ranging from ACN to TOL). Therefore, we propose that the electron donor/acceptor dyads with two identical chromophores showing the symmetry breaking spin orbit charge transfer induced ISC will be helpful for design of triplet PSs showing high triplet state energy levels.

3. Conclusion

In summary, we studied the relationship between the molecular geometry, and the electronic coupling between the two anthryl units between the 9,9'-bianthryl and 2,9'-bianthryl, and the spin orbit charge transfer efficiency (SOCT-ISC). We found that the effect of the molecular geometry on the photophysical properties, i.e. lower fluorescence quantum yields, more significant solvent polarity-dependency and longer fluorescence lifetime and higher SOCT-ISC efficiency for 9,9'-bianthryl, which is with orthogonal geometry, in comparison with 2,9'-bianthryl which is with more coplanar geometry. Efficient ISC in BAs was confirmed with nanosecond transient absorption spectroscopy, and the triplet state lifetime are long (9,9'-bianthryl, $\tau_T = 353 \mu\text{s}$, 2,9'-bianthryl, $\tau_T = 493 \mu\text{s}$ in ACN).



Scheme 2. Simplified Jablonski Diagram Illustrating the Photophysical Processes Involved in (a) 9,9'-BA and (b) 2,9'-BA. The energy levels of the excited state are derived from the spectroscopic and electrochemical study data, and the energy levels of the triplet states are from TDDFT//B3LYP/6-31G (d) with Gaussian 09W.

4. Experimental section

4.1. Materials and equipment

All the chemicals used for synthesis are analytically pure and were used as received. Petroleum ether (boiling point: 60–90 °C) was used for

column chromatography. UV-Vis absorption spectra were taken on a UV-2550 UV-vis spectrophotometer (Shimadzu Ltd, Japan). Fluorescence spectra were obtained on a RF-5301PC spectrofluorometer (Shimadzu Ltd, Japan). Fluorescence lifetimes were measured on an OB920 (Edinburgh Instruments Ltd, UK) luminescence lifetime spectrometer (Time correlated single photon counting, TCSPC detection mode).

4.2. Synthesis of 9,9'-BA

9,9'-BA was synthesized with a modified literature method [103]. Acetic acid (19 mL) was added in the mixture of anthraquinone (784.5 mg, 3.75 mmol) and zinc powder (1.96 g, 30 mmol). Under N₂ atmosphere, 37% HCl solution (4.7 mL) was added slowly with dropping funnel at 50 °C. The reaction mixture was refluxed for 13 h. Then the heating source bath was removed and the mixture was cooled to room temperature (RT). After the mixture was filtered, the filter residue was washed with methanol, and then was re-dissolved in chloroform (4 mL). Then the mixture was added to ethanol (50 mL). The precipitate was filtered to give a crude product. The crude product was further purified with column chromatography (silica gel, 2–4% CH₂Cl₂ in petroleum ether, v/v) to give a beige solid (69 mg, yield: 10%). M.p.: > 250 °C. ¹H NMR (400 MHz, CDCl₃): δ = 8.69 (s, 2H), 8.16 (d, *J* = 8.5 Hz, 4H), 7.47–7.43 (m, 4H), 7.17–7.07 (m, 8H). HRMS (EI): Calcd ([C₂₈H₁₈]⁺), *m/z* = 354.1410; found, *m/z* = 354.1409.

4.3. Synthesis of 2,9'-BA

A solution of 9-bromoanthracene (128 mg, 0.5 mmol) in TOL (10 mL) was mixed with a solution of 2-anthraceneboronic acid (105 mg, 0.47 mmol) in ethanol (6 mL). Then an aqueous solution of K₂CO₃ (2.1 mL, 2 M) was added. The suspension was bubbled with nitrogen for 30 min and Pd(PPh₃)₄ (14 mg, 0.012 mmol) was then added. Kept in darkness, the reaction mixture was stirred at 100 °C under N₂ atmosphere for 8 h. After completion of the reaction, the reaction mixture was cooled to RT. Then water (30 mL) was added. The mixture was extracted with CH₂Cl₂ (3 × 50 mL). The combined organic layers were dried over anhydrous Na₂SO₄ and filtered. Then the solvent was evaporated under reduced pressure to obtain a crude solid. The crude product was further purified with column chromatography (silica gel, petroleum ether) to give a pale yellow solid (128 mg, yield: 77%). M.p.: 230–233 °C. ¹H NMR (400 MHz, CDCl₃): δ = 8.59 (d, *J* = 13.9 Hz, 2H), 8.48 (s, 1H), 8.22 (d, *J* = 8.5 Hz, 1H), 8.10–8.03 (m, 5H), 7.77 (d, *J* = 8.7 Hz, 2H), 7.56–7.46 (m, 5H), 7.36–7.32 (m, 2H). ¹³C NMR (126 MHz, CDCl₃): δ = 136.8, 135.7, 132.1, 132.0, 131.5, 131.4, 131.0, 130.3, 130.2, 129.3, 128.4, 128.2, 128.1, 126.8, 126.7, 126.4, 126.2, 125.6, 125.5, 125.2. HRMS (EI): Calcd ([C₂₈H₁₈]⁺), *m/z* = 354.1400; found, *m/z* = 354.1409.

4.4. Nanosecond transient absorption spectroscopy

The ns TA spectra were studied on a LP920 laser flash-photolysis spectrometer (Edinburgh Instruments Ltd, U.K.), and the signal was digitized with a Tektronix TDS 3012B oscilloscope. The data (kinetic decay curve and spectrum) were analyzed with the L900 software. All samples for the nanosecond transient absorption measurements were deaerated with N₂ for about 15 min before measurement, and the cuvette was sealed during the measurement.

4.5. Density Functional Theory calculations

The geometries of the compounds were optimized using DFT with B3LYP functional and 6-31G(d) basis set. Compared to the results of BA dyads calculated by CAM-B3LYP functional, the results from B3LYP functional show CT absorption in 422 nm (Table S1 and Table S2). Although it is not distinct in UV–Visible absorption spectrum due to the orthogonal geometry at ground state, the results are consistent with the fluorescence changes in different polarity solvents, which are the feature of CT state. Thus, B3LYP functional is more appropriate for BAs system. There are no imaginary frequencies for all optimized structures. The excitation energy and the energy gaps between the S₀ state and the triplet excited states of the compounds were approximated based on the optimal ground-state geometry. The T₁→T_n absorption calculation of 9,9'-BA, 2,9'-BA and An are based on the optimal T₁ state geometry

calculated by TDDFT//B3LYP/6-31G (d), which is similar to the calculation of normal UV–Vis spectra. All these calculations were performed with Gaussian 09W [104].

CRedit authorship contribution statement

Xiaoyu Zhao: synthesized the compounds, performed spectral measurement and prepared part of the manuscript. **Andrey A. Sukhanov:** data analysis. **KePeng Chen:** parts of synthesis and spectral data analysis. **Xinyu Geng:** parts of synthesis and spectral data analysis. **Yu Dong:** parts of synthesis and spectral data analysis. **Violeta K. Voronkova:** parts of spectral data analysis. **Jianzhang Zhao:** conceived the project, analyzed the data and wrote the manuscript. **Lang Liu:** parts of spectral data analysis.

Declaration of competing interest

The authors declare that they have no known competing financial interests or personal relationships that could have appeared to influence the work reported in this paper.

Acknowledgement

J. Z. thanks the NSFC (U2001222, 21673031, 21761142005, and 21911530095), the State Key Laboratory of Fine Chemicals (ZYTS201901), Xinjiang University and the Department of Education of the Xinjiang Uyghur Autonomous Region (TianShan Chair Professor) for financial support.

Appendix A. Supplementary data

Supplementary data to this article can be found online at <https://doi.org/10.1016/j.dyepig.2020.109121>.

References

- [1] Shi L, Xia W. Photoredox functionalization of C–H bonds adjacent to a nitrogen atom. *Chem Soc Rev* 2012;41:7687–97. <https://doi.org/10.1039/c2cs35203f>.
- [2] Fukuzumi S, Ohkubo K. Selective photocatalytic reactions with organic photocatalysts. *Chem Sci* 2013;4:561–74. <https://doi.org/10.1039/c2sc21449k>.
- [3] Hari DP, König B. The photocatalyzed Meerwein arylation: classic reaction of aryl diazonium salts in a new light. *Angew Chem Int Ed* 2013;52:4734–43. <https://doi.org/10.1002/anie.201210276>.
- [4] Hari DP, König B. Synthetic applications of eosin Y in photoredox catalysis. *Chem Commun* 2014;50:6688–99. <https://doi.org/10.1039/c4cc00751d>.
- [5] Dai FR, Zhan HM, Liu Q, Fu YY, Li JH, Wang QW, Xie Z, Wang L, Yan F, Wong WY. Platinum(II)-bis(aryleneethynylene) complexes for solution-processible molecular bulk heterojunction solar cells. *Chem Eur J* 2012;18:1502–11. <https://doi.org/10.1002/chem.201102598>.
- [6] Suzuki S, Matsumoto Y, Tsubamoto M, Sugimura R, Kozaki M, Kimoto K, Iwamura M, Nozaki K, Senju N, Uragami C, Hashimoto H, Muramatsu Y, Konno A, Okada K. Photoinduced electron transfer of platinum(II) bipyridine diacetylides linked by triphenylamine- and naphthaleneimide-derivatives and their application to photoelectric conversion systems. *Phys Chem Chem Phys* 2013;15:8088–94. <https://doi.org/10.1039/c3cp50182e>.
- [7] Awuah SG, You Y. Boron dipyrromethene (BODIPY)-based photosensitizers for photodynamic therapy. *RSC Adv* 2012;2:11169–83. <https://doi.org/10.1039/c2ra21404k>.
- [8] Kamkaew A, Lim SH, Lee HB, Kiew LV, Chung LY, Burgess K. BODIPY dyes in photodynamic therapy. *Chem Soc Rev* 2013;42:77–88. <https://doi.org/10.1039/c2cs35216h>.
- [9] Stacey OJ, Pope SJA. New avenues in the design and potential application of metal complexes for photodynamic therapy. *RSC Adv* 2013;3:25550–64. <https://doi.org/10.1039/c3ra45219k>.
- [10] Zhao J, Wu W, Sun J, Guo S. Triplet photosensitizers: from molecular design to applications. *Chem Soc Rev* 2013;42:5323–51. <https://doi.org/10.1039/c3cs35531d>.
- [11] Li X, Koleman S, Yoon J, Akkaya EU. Activatable photosensitizers: agents for selective photodynamic therapy. *Adv Funct Mater* 2017;27:1604053. <https://doi.org/10.1002/adfm.201604053>.
- [12] Ceroni P. Energy up-conversion by low-power excitation: new applications of an old concept. *Chem Eur J* 2011;17:9560–4. <https://doi.org/10.1002/chem.201101102>.

- [13] Zhao J, Ji S, Guo H. Triplet–triplet annihilation based upconversion: from triplet sensitizers and triplet acceptors to upconversion quantum yields. *RSC Adv* 2011; 1:937–50. <https://doi.org/10.1039/c1ra00469g>.
- [14] Simon YC, Weder C. Low-power photon upconversion through triplet–triplet annihilation in polymers. *J Mater Chem* 2012;22:20817–30. <https://doi.org/10.1039/c2jm33654e>.
- [15] Ye C, Zhou L, Wang X, Liang Z. Photon upconversion: from two-photon absorption (TPA) to triplet–triplet annihilation (TTA). *Phys Chem Chem Phys* 2016;18:10818–35. <https://doi.org/10.1039/c5cp07296d>.
- [16] Yanai N, Kimizuka N. New triplet sensitization routes for photon upconversion: thermally activated delayed fluorescence molecules, inorganic nanocrystals, and singlet-to-triplet absorption. *Acc Chem Res* 2017;50:2487–95. <https://doi.org/10.1021/acs.accounts.7b00235>.
- [17] Turro NJ, Scaiano JC, Ramamurthy V. *Principles of molecular photochemistry: an introduction*. Sausalito, CA: University Science Books; 2009.
- [18] Gorman A, Killoran J, O'Shea C, Kenna T, Gallagher WM, O'Shea DF. In vitro demonstration of the heavy-atom effect for photodynamic therapy. *J Am Chem Soc* 2004;126:10619–31. <https://doi.org/10.1021/ja047649e>.
- [19] Yogo T, Urano Y, Ishitsuka Y, Maniwa F, Nagano T. Highly efficient and photostable photosensitizer based on BODIPY chromophore. *J Am Chem Soc* 2005;127:12162–3. <https://doi.org/10.1021/ja0528533>.
- [20] Wong WY, Ho CL. Di-, oligo- and polymetallaynes: syntheses, photophysics, structures and applications. *Coord Chem Rev* 2006;250:2627–90. <https://doi.org/10.1016/j.ccr.2006.04.014>.
- [21] Sabatini RP, McCormick TM, Lazarides T, Wilson KC, Eisenberg R, McCamant DW. Intersystem crossing in halogenated bodipy chromophores used for solar hydrogen production. *J Phys Chem Lett* 2011;2:223–7. <https://doi.org/10.1021/jz101697y>.
- [22] Zhang XF, Yang X. Singlet oxygen generation and triplet excited-state spectra of brominated BODIPY. *J Phys Chem B* 2013;117:5533–9. <https://doi.org/10.1021/jp4013812>.
- [23] Flamigni L, Barbieri A, Sabatini C, Ventura B, Barigelletti F. *Photochemistry and photophysics of coordination compounds: Iridium*. Berlin, Heidelberg: Springer Berlin Heidelberg; 2007. p. 143–203.
- [24] Zhao Q, Li F, Huang C. Phosphorescent chemosensors based on heavy-metal complexes. *Chem Soc Rev* 2010;39:3007–30. <https://doi.org/10.1039/b915340c>.
- [25] Chou PT, Chi Y, Chung MW, Lin CC. Harvesting luminescence via harnessing the photophysical properties of transition metal complexes. *Coord Chem Rev* 2011; 255:2653–65. <https://doi.org/10.1016/j.ccr.2010.12.013>.
- [26] Feng Y, Cheng J, Zhou L, Zhou X, Xiang H. Ratiometric optical oxygen sensing: a review in respect of material design. *Analyst* 2012;137:4885–901. <https://doi.org/10.1039/c2an35907c>.
- [27] You Y, Nam W. Photofunctional triplet excited states of cyclometalated Ir(III) complexes: beyond electroluminescence. *Chem Soc Rev* 2012;41:7061–84. <https://doi.org/10.1039/c2cs35171d>.
- [28] Liu Z, He W, Guo Z. Metal coordination in photoluminescent sensing. *Chem Soc Rev* 2013;42:1568–600. <https://doi.org/10.1039/c2cs35363f>.
- [29] Rajagopal SK, Mallia AR, Hariharan M. Enhanced intersystem crossing in carbonylpyrenes. *Phys Chem Chem Phys* 2017;19:28225–31. <https://doi.org/10.1039/c7cp04834c>.
- [30] Bröring M, Krüger R, Link S, Kleeberg C, Köhler S, Xie X, Ventura B, Flamigni L. Bis(BF₂)-2,2'-bidipyrins (BisBODIPYs): highly fluorescent BODIPY dimers with large Stokes shifts. *Chem Eur J* 2008;14:2976–83. <https://doi.org/10.1002/chem.200701912>.
- [31] Ventura B, Marconi G, Bröring M, Krüger R, Flamigni L. Bis(BF₂)-2,2'-bidipyrins, a class of BODIPY dyes with new spectroscopic and photophysical properties. *New J Chem* 2009;33:428–38. <https://doi.org/10.1039/b813638f>.
- [32] Amin AN, El-Khouly ME, Subbaiyan NK, Zandler ME, Fukuzumi S, D'Souza F. A novel BF₂-chelated azadipyrromethene–fullerene dyad: synthesis, electrochemistry and photodynamics. *Chem Commun* 2012;48:206–8. <https://doi.org/10.1039/c1cc16071k>.
- [33] Huang L, Yu X, Wu W, Zhao J. Styryl bodipy-C₆₀ dyads as efficient heavy-atom-free organic triplet photosensitizers. *Org Lett* 2012;14:2594–7. <https://doi.org/10.1021/ol3008843>.
- [34] Verhoeven JW, van Ramesdonk HJ, Groeneveld MM, Benniston AC, Harriman A. Long-lived charge-transfer states in compact donor–acceptor dyads. *ChemPhysChem* 2005;6:2251–60. <https://doi.org/10.1002/cphc.200500029>.
- [35] Verhoeven JW. On the role of spin correlation in the formation, decay, and detection of long-lived, intramolecular charge-transfer states. *J Photochem Photobiol C Photochem Rev* 2006;7:40–60. <https://doi.org/10.1016/j.jphotochemrev.2006.04.001>.
- [36] Ziesel R, Allen BD, Rewinska DB, Harriman A. Selective triplet-state formation during charge recombination in a fullerene/bodipy molecular dyad (bodipy=borondipyrromethene). *Chem Eur J* 2009;15:7382–93. <https://doi.org/10.1002/chem.200900440>.
- [37] Vauthey E. Photoinduced symmetry-breaking charge separation. *ChemPhysChem* 2012;13:2001–11. <https://doi.org/10.1002/cphc.201200106>.
- [38] Kc CB, Lim GN, Nesterov VN, Karr PA, D'Souza F. Phenothiazine–BODIPY–Fullerene triads as photosynthetic reaction center models: substitution and solvent polarity effects on photoinduced charge separation and recombination. *Chem Eur J* 2014;20:17100–12. <https://doi.org/10.1002/chem.201404863>.
- [39] Guldi DM. Fullerenes: three dimensional electron acceptor materials. *Chem Commun* 2000:321–7. <https://doi.org/10.1039/a907807j>.
- [40] Chen KY, Hsieh CC, Cheng YM, Lai CH, Chou PT, Chow TJ. Tuning excited-state electron transfer from an adiabatic to nonadiabatic type in donor–bridge–acceptor systems and the associated energy-transfer process. *J Phys Chem A* 2006;110:12136–44. <https://doi.org/10.1021/jp063038s>.
- [41] Wiederrecht GP, Svec WA, Wasielewski MR, Gallili T, Levanon H. Novel mechanism for triplet state formation in short distance covalently linked radical ion pairs. *J Am Chem Soc* 2000;122:9715–22. <https://doi.org/10.1021/ja000662o>.
- [42] Weiss EA, Ratner MA, Wasielewski MR. Direct measurement of singlet–triplet splitting within rodlike photogenerated radical ion pairs using magnetic field effects: estimation of the electronic coupling for charge recombination. *J Phys Chem A* 2003;107:3639–47. <https://doi.org/10.1021/jp0224315>.
- [43] Dance ZEX, Mi Q, McCamant DW, Ahrens MJ, Ratner MA, Wasielewski MR. Time-resolved EPR studies of photogenerated radical ion pairs separated by p-phenylene oligomers and of triplet states resulting from charge recombination. *J Phys Chem B* 2006;110:25163–73. <https://doi.org/10.1021/jp063690n>.
- [44] Veldman D, Chopin SMA, Meskers SCJ, Janssen RAJ. Enhanced intersystem crossing via a high energy charge transfer state in a perylenediimide–perylene monoimide dyad. *J Phys Chem A* 2008;112:8617–32. <https://doi.org/10.1021/jp805949r>.
- [45] Okada T, Karaki I, Matsuzawa E, Mataga N, Sakata Y, Misumi S. Ultrafast intersystem crossing in some intramolecular heteroexcimers. *J Phys Chem* 1981; 85:3957–60. <https://doi.org/10.1021/j150626a002>.
- [46] van Willigen H, Jones G, Farahat MS. Time-resolved EPR study of photoexcited triplet-state formation in electron-donor-substituted acridinium ions. *J Phys Chem* 1996;100:3312–6. <https://doi.org/10.1021/jp953176+>.
- [47] Harriman A, Mallon LJ, Ulrich G, Ziesel R. Rapid intersystem crossing in closely spaced but orthogonal molecular dyads. *ChemPhysChem* 2007;8:1207–14. <https://doi.org/10.1002/cphc.200700060>.
- [48] Dance ZEX, Mickleby SM, Wilson TM, Ricks AB, Scott AM, Ratner MA, Wasielewski MR. Intersystem crossing mediated by photoinduced intramolecular charge transfer: julolidine–anthracene molecules with perpendicular π systems. *J Phys Chem A* 2008;112:4194–201. <https://doi.org/10.1021/jp800561g>.
- [49] Epelde-Elezcano N, Palao E, Manzano H, Prieto-Castañeda A, Agarrabeitia AR, Tabero A, Villanueva A, de la Moya S, López-Arbeloa Í, Martínez-Martínez V, Ortiz MJ. Rational design of advanced photosensitizers based on orthogonal BODIPY dimers to finely modulate singlet oxygen generation. *Chem Eur J* 2017; 23:4837–48. <https://doi.org/10.1002/chem.201605822>.
- [50] Pilatov MA, Karuthedath S, Polestshuk PM, Savoie H, Flanagan KJ, Sy C, Sitte E, Telitshko M, Laquai F, Boyle RW, Senge MO. Generation of triplet excited states via photoinduced electron transfer in meso-anthra-BODIPY: fluorogenic response toward singlet oxygen in solution and in vitro. *J Am Chem Soc* 2017;139:6282–5. <https://doi.org/10.1021/jacs.7b00551>.
- [51] Wang Z, Zhao J. Bodipy–anthracene dyads as triplet photosensitizers: effect of chromophore orientation on triplet-state formation efficiency and application in triplet–triplet annihilation upconversion. *Org Lett* 2017;19:4492–5. <https://doi.org/10.1021/acs.orglett.7b02047>.
- [52] Chen K, Yang W, Wang Z, Iagatti A, Bussotti L, Foggi P, Ji W, Zhao J, Donato MD. Triplet excited state of BODIPY accessed by charge recombination and its application in triplet–triplet annihilation upconversion. *J Phys Chem A* 2017;121: 7550–64. <https://doi.org/10.1021/acs.jpca.7b07623>.
- [53] Zhang XF, Feng N. Photoinduced electron transfer-based halogen-free photosensitizers: covalent meso-aryl (phenyl, naphthyl, anthryl, and pyrenyl) as electron donors to effectively induce the formation of the excited triplet state and singlet oxygen for BODIPY compounds. *Chem Asian J* 2017;12:2447–56. <https://doi.org/10.1002/asia.201700794>.
- [54] Imran M, Sukhanov AA, Wang Z, Karatay A, Zhao J, Mahmood Z, Elmali A, Voronkova VK, Hayvali M, Xing Y, Weber S. Electronic coupling and spin–orbit charge-transfer intersystem crossing in phenothiazine–perylene compact electron donor/acceptor dyads. *J Phys Chem C* 2019;123:7010–24. <https://doi.org/10.1021/acs.jpcc.8b12040>.
- [55] Zhao Y, Duan R, Zhao J, Li C. Spin–orbit charge transfer intersystem crossing in perylenemonoimide–phenothiazine compact electron donor–acceptor dyads. *Chem Commun* 2018;54:12329–32. <https://doi.org/10.1039/c8cc07012a>.
- [56] Hou Y, Biskup T, Rein S, Wang Z, Bussotti L, Russo N, Foggi P, Zhao J, Donato MD, Mazzone G, Weber S. Spin–orbit charge recombination intersystem crossing in phenothiazine–anthracene compact dyads: effect of molecular conformation on electronic coupling, electronic transitions, and electron spin polarizations of the triplet states. *J Phys Chem C* 2018;122:27850–65. <https://doi.org/10.1021/acs.jpcc.8b08965>.
- [57] Dong Y, Sukhanov AA, Zhao J, Elmali A, Li X, Dick B, Karatay A, Voronkova VK. Spin–orbit charge-transfer intersystem crossing (SOCT-ISC) in bodipy–phenoxazine dyads: effect of chromophore orientation and conformation restriction on the photophysical properties. *J Phys Chem C* 2019;123:22793–811. <https://doi.org/10.1021/acs.jpcc.9b06170>.
- [58] Mataga N, Yao H, Okada T, Rettig W. Charge-transfer rates in symmetric and symmetry-disturbed derivatives of 9,9'-bianthryl. *J Phys Chem* 1989;93:3383–6. <https://doi.org/10.1021/j100346a004>.
- [59] Grabner G, Rechthaler K, Köhler G. Two-state model for the photophysics of 9,9'-bianthryl. Fluorescence, transient-absorption, and semiempirical studies. *J Phys Chem A* 1998;102:689–96. <https://doi.org/10.1021/jp9727815>.
- [60] Grabowski ZR, Rotkiewicz K, Rettig W. Structural changes accompanying intramolecular electron transfer: focus on twisted intramolecular charge-transfer states and structures. *Chem Rev* 2003;103:3899–4032. <https://doi.org/10.1021/cr940745l>.
- [61] Takaya T, Saha S, Hamaguchi H-o, Sarkar M, Samanta A, Iwata K. Charge resonance character in the charge transfer state of bianthryls: effect of symmetry

- breaking on time-resolved near-IR absorption spectra. *J Phys Chem A* 2006;110:4291–5. <https://doi.org/10.1021/jp060049c>.
- [62] Lee C, Choi CH, Joo T. A solvent–solute cooperative mechanism for symmetry-breaking charge transfer. *Phys Chem Chem Phys* 2020;22:1115–21. <https://doi.org/10.1039/c9cp05090f>.
- [63] Yu Y, Wu Z, Li Z, Jiao B, Li L, Ma L, Wang D, Zhou G, Hou X. Highly efficient deep-blue organic electroluminescent devices ($CIE_y \approx 0.08$) doped with fluorinated 9,9'-bianthracene derivatives (fluorophores). *J Mater Chem C* 2013;1:8117–27. <https://doi.org/10.1039/c3tc31743a>.
- [64] Pu YJ, Satake R, Koyama Y, Otomo T, Hayashi R, Haruta N, Katagiri H, Otsuki D, Kim D, Sato T. Absence of delayed fluorescence and triplet–triplet annihilation in organic light emitting diodes with spatially orthogonal bianthracenes. *J Mater Chem C* 2019;7:2541–7. <https://doi.org/10.1039/c8tc05817b>.
- [65] Liu H, Yan X, Shen L, Tang Z, Liu S, Li X. Color-tunable upconversion emission from a twisted intramolecular charge-transfer state of anthracene dimers via triplet–triplet annihilation. *Mater Horiz* 2019;6:990–5. <https://doi.org/10.1039/c8mh01586d>.
- [66] Catalán J, Díaz C, López V, Pérez P, Claramunt RM. The TICT mechanism in 9,9'-biaryl compounds: solvatochromism of 9,9'-bianthryl, *N*-(9-anthryl)carbazole, and *N,N'*-bicarbazyl. *J Phys Chem* 1996;100:18392–8. <https://doi.org/10.1021/jp9612590>.
- [67] Hou Y, Zhang X, Chen K, Liu D, Wang Z, Liu Q, Zhao J, Barbon A. Charge separation, charge recombination, long-lived charge transfer state formation and intersystem crossing in organic electron donor/acceptor dyads. *J Mater Chem C* 2019;7:12048–74. <https://doi.org/10.1039/c9tc04285g>.
- [68] Das S, Thornbury WG, Bartynski AN, Thompson ME, Bradforth SE. Manipulating triplet yield through control of symmetry-breaking charge transfer. *J Phys Chem Lett* 2018;9:3264–70. <https://doi.org/10.1021/acs.jpclett.8b01237>.
- [69] Catalán J, Díaz C, López V, Pérez P, Claramunt RM. On the TICT mechanism of 9,9'-biaryl compounds. *Eur J Org Chem* 1998;1998:1697–704. [https://doi.org/10.1002/\(SICI\)1099-0690\(199808\)1998:8<1697::AID-EJOC1697>3.0.CO;2-W](https://doi.org/10.1002/(SICI)1099-0690(199808)1998:8<1697::AID-EJOC1697>3.0.CO;2-W).
- [70] Evers F, Giraud-Girard J, Grimme S, Manz J, Monte C, Oettel M, Rettig W, Saalfrank P, Zimmermann P. Absorption and fluorescence excitation spectra of 9-(*N*-carbazolyl)-anthracene: effects of intramolecular vibrational redistribution and diabatic transitions involving electron transfer. *J Phys Chem A* 2001;105:2911–24. <https://doi.org/10.1021/jp003879d>.
- [71] Piet JJ, Schuddeboom W, Wegewijs BR, Grozema FC, Warman JM. Symmetry breaking in the relaxed S_1 excited state of bianthryl derivatives in weakly polar solvents. *J Am Chem Soc* 2001;123:5337–47. <https://doi.org/10.1021/ja004341o>.
- [72] Wortmann R, Lebus S, Elich K, Assar S, Detzer N, Liptay W. Solvent dependence of effective S_1 torsional potentials in 9,9'-bianthryl and 9-phenylanthracene. *Chem Phys Lett* 1992;198:220–8. [https://doi.org/10.1016/0009-2614\(92\)90076-Y](https://doi.org/10.1016/0009-2614(92)90076-Y).
- [73] Yamasaki K, Arita K, Kajimoto O, Hara K. The torsional potential of 9,9'-bianthryl determined by laser-induced fluorescence in a free jet. *Chem Phys Lett* 1986;123:277–81. [https://doi.org/10.1016/0009-2614\(86\)80072-0](https://doi.org/10.1016/0009-2614(86)80072-0).
- [74] Asami N, Takaya T, Yabumoto S, Shigeto S, Hamaguchi H-o, Iwata K. Two different charge transfer states of photoexcited 9,9'-bianthryl in polar and nonpolar solvents characterized by nanosecond time-resolved near-IR spectroscopy in the 4500–10 500 cm^{-1} region. *J Phys Chem A* 2010;114:6351–5. <https://doi.org/10.1021/jp912173h>.
- [75] Lakowicz JR. *Principles of fluorescence spectroscopy*. third ed. New York: Kluwer Academic; 2006.
- [76] Jurczok M, Plaza P, Martin MM, Meyer YH, Rettig W. Excited state relaxation paths in 9,9'-bianthryl and 9-carbazolyl-anthracene: a sub-ps transient absorption study. *Chem Phys* 2000;253:339–49. [https://doi.org/10.1016/S0301-0104\(99\)00386-9](https://doi.org/10.1016/S0301-0104(99)00386-9).
- [77] Rettig W, Zander M. Broken symmetry in excited states of 9,9'-bianthryl. *Ber Bunsen Ges Phys Chem* 1983;87:1143–9. <https://doi.org/10.1002/bbpc.19830871212>.
- [78] Müller S, Heinze J. Fluorescence analysis of two new TICT systems: 10-cyano-9,9'-bianthryl (CBA) and 10,10'-dicyano-9,9'-bianthryl (DCBA). *Chem Phys* 1991;157:231–42. [https://doi.org/10.1016/0301-0104\(91\)87147-N](https://doi.org/10.1016/0301-0104(91)87147-N).
- [79] Verhoeven JW, Scherer T, Wegewijs B, Hermant RM, Jortner J, Bixon M, Depaemelaere S, de Schryver FC. Electronic coupling in inter- and intramolecular donor-acceptor systems as revealed by their solvent-dependent charge-transfer fluorescence. *Recl Trav Chim Pays-Bas* 1995;114:443–8. <https://doi.org/10.1002/recl.19951141104>.
- [80] Schütz M, Schmidt R. Deactivation of 9,9'-bianthryl in solution studied by photoacoustic calorimetry and fluorescence. *J Phys Chem* 1996;100:2012–8. <https://doi.org/10.1021/jp951193t>.
- [81] Li W, Liu D, Shen F, Ma D, Wang Z, Feng T, Xu Y, Yang B, Ma Y. A twisting donor-acceptor molecule with an intercrossed excited state for highly efficient, deep-blue electroluminescence. *Adv Punct Mater* 2012;22:2797–803. <https://doi.org/10.1002/adfm.201200116>.
- [82] Mohammed OF, Vauthey E. Ultrafast excited-state dynamics of aminopyrene and of its protonated form observed by femtosecond absorption spectroscopy. *Chem Phys Lett* 2010;487:246–50. <https://doi.org/10.1016/j.cplett.2010.01.066>.
- [83] Hamanoue K, Hidaka T, Nakayama T, Teranishi H, Sumitani M, Yoshihara K. Solvent effects on the nonradiative relaxation processes of the lowest excited singlet states of meso-substituted bromoanthracenes. *Bull Chem Soc Jpn* 1983;56:1851–2. <https://doi.org/10.1246/bcsj.56.1851>.
- [84] Kanamaru N. Radiationless transition between randomly fluctuating levels. S_1 - T_2 - T_1 intersystem crossing in condensed phase. *Bull Chem Soc Jpn* 1982;55:3093–6. <https://doi.org/10.1246/bcsj.55.3093>.
- [85] Wilkinson F, McGarvey DJ, Olea AF. Factors governing the efficiency of singlet oxygen production during oxygen quenching of singlet and triplet states of anthracene derivatives in cyclohexane solution. *J Am Chem Soc* 1993;115:12144–51. <https://doi.org/10.1021/ja00078a062>.
- [86] Kamata Y, Akiyama K, Tero-Kubota S. Anisotropic intersystem crossing from the upper excited triplet states of anthracenes: two-laser time-resolved EPR study. *J Phys Chem A* 1999;103:1714–8. <https://doi.org/10.1021/jp983916p>.
- [87] Mortensen J, Heinze J, Herbst H, Müllen K. Electrochemical generation of highly reduced oligoanthrylene systems ϵ -a voltammetric study. *J Electroanal Chem* 1992;324:201–17. [https://doi.org/10.1016/0022-0728\(92\)80046-7](https://doi.org/10.1016/0022-0728(92)80046-7).
- [88] Xu K, Zhao J, Escudero D, Mahmood Z, Jacquemin D. Controlling triplet–triplet annihilation upconversion by tuning the pet in aminomethyleneanthracene derivatives. *J Phys Chem C* 2015;119:23801–12. <https://doi.org/10.1021/acs.jpcc.5b05325>.
- [89] Shi W, El-Khouly ME, Ohkubo K, Fukuzumi S, Ng DKP. Photosynthetic antenna-reaction center mimicry with a covalently linked monostyryl boron-dipyrromethene-aza-boron-dipyrromethene- C_{60} triad. *Chem Eur J* 2013;19:11332–41. <https://doi.org/10.1002/chem.201300318>.
- [90] Wang Z, Sukhanov AA, Toffoletti A, Sadiq F, Zhao J, Barbon A, Voronkova VK, Dick B. Insights into the efficient intersystem crossing of bodipy-anthracene compact dyads with steady-state and time-resolved optical/magnetic spectroscopies and observation of the delayed fluorescence. *J Phys Chem C* 2019;123:265–74. <https://doi.org/10.1021/acs.jpcc.8b10835.s001>.
- [91] Balazs GC, del Guerro A, Schmeihl RH. Photophysical behavior and intramolecular energy transfer in Os(II) diimine complexes covalently linked to anthracene. *Photochem Photobiol Sci* 2005;4:89–94. <https://doi.org/10.1039/b410472m>.
- [92] Carmichael I, Hug GL. Triplet–triplet absorption spectra of organic molecules in condensed phases. *J Phys Chem Ref Data* 1986;15:1–250. <https://doi.org/10.1063/1.555770>.
- [93] Yildiz A, Reilly CN. The mechanism of intersystem crossing for some substituted aromatic hydrocarbons. *Spectrosc Lett* 1968;1:335–43. <https://doi.org/10.1080/00387016808404986>.
- [94] Hunter TF, Wyatt RF. Intersystem crossing in anthracene. *Chem Phys Lett* 1970;6:221–4. [https://doi.org/10.1016/0009-2614\(70\)80224-X](https://doi.org/10.1016/0009-2614(70)80224-X).
- [95] Wang X, Goeb S, Ji Z, Castellano FN. Excited state absorption properties of Pt(II) terpyridyl complexes bearing π -conjugated arylacetylides. *J Phys Chem B* 2010;114:14440–9. <https://doi.org/10.1021/jp101528z>.
- [96] Phillips KA, Stonelake TM, Chen K, Hou Y, Zhao J, Coles SJ, Horton PN, Keane SJ, Stokes EC, Fallis IA, Hallett AJ, O'Kell SP, Beames JM, Pope SJA. Ligand-tunable, red-emitting iridium(III) complexes for efficient triplet–triplet annihilation upconversion performance. *Chem Eur J* 2018;24:8577–88. <https://doi.org/10.1002/chem.201801007>.
- [97] Grozema FC, Swart M, Zijlstra RWJ, Piet JJ, Siebbeles LDA, van Duijn PT. QM/MM study of the role of the solvent in the formation of the charge separated excited state in 9,9'-bianthryl. *J Am Chem Soc* 2005;127:11019–28. <https://doi.org/10.1021/ja051729g>.
- [98] Gramp P, Kapturkiewicz A, Salbeck J. Nature of 9,9'-bianthryl and 10,10'-dimethoxy-9,9'-bianthryl radical anions. *Chem Phys* 1994;187:391–7. [https://doi.org/10.1016/0301-0104\(94\)89021-8](https://doi.org/10.1016/0301-0104(94)89021-8).
- [99] Takaya T, Hamaguchi H-o, Kuroda H, Iwata K. Femtosecond electron transfer dynamics of 9,9'-bianthryl in acetonitrile as studied by time-resolved near-infrared absorption spectroscopy. *Chem Phys Lett* 2004;399:210–4. <https://doi.org/10.1016/j.cplett.2004.09.148>.
- [100] Tanaka F, Okamoto M, Hirayama S. Pressure and temperature dependences of the rate constant for S_1 - T_2 intersystem crossing of anthracene compounds in solution. *J Phys Chem* 1995;99:525–30. <https://doi.org/10.1021/j100002a013>.
- [101] Metz F. Position-dependent deuterium effect on relative rate constants for isc processes in aromatic hydrocarbons. *Chem Phys Lett* 1973;22:186–90. [https://doi.org/10.1016/0009-2614\(73\)80567-6](https://doi.org/10.1016/0009-2614(73)80567-6).
- [102] Widman RP, Huber JR. Temperature effects in the intersystem crossing process of anthracene. *J Phys Chem* 1972;76:1524–7. <https://doi.org/10.1021/j100655a005>.
- [103] Lee H, Jo M, Yang G, Jung H, Kang S, Park J. Highly efficient dual anthracene core derivatives through optimizing size groups for blue emission. *Dyes Pigments* 2017;146:27–36. <https://doi.org/10.1016/j.dyepig.2017.06.053>.
- [104] Frisch MJ, Trucks GW, Schlegel HB, Scuseria GE, Robb MA, Cheeseman JR, et al. *Gaussian 09w* (revision A.01). Wallingford CT: Gaussian Inc; 2016.